

1 **CHANS-SD-YRB V1.0: A System Dynamics model of**  
2 **the coupled human-natural systems for the Yellow**  
3 **River Basin**

4 Shan Sang<sup>1,2</sup>, Yan Li<sup>1,2\*</sup>, Shuang Zong<sup>1,2</sup>, Lu Yu<sup>1,2</sup>, Shuai Wang<sup>1,2</sup>, Yanxu Liu<sup>1,2</sup>,  
5 Xutong Wu<sup>1,2</sup>, Shuang Song<sup>1,2</sup>, Wenwu Zhao<sup>1,2</sup>, Xuhui Wang<sup>3</sup>, Bojie Fu<sup>4</sup>

6 <sup>1</sup>State Key Laboratory of Earth Surface Processes and Hazards Risk Governance (ESPHR), Beijing  
7 Normal University, Beijing, China

8 <sup>2</sup>Institute of Land Surface System and Sustainable Development, Faculty of Geographical Science,  
9 Beijing Normal University, Beijing, China

10 <sup>3</sup>Institute of Carbon Neutrality, Laboratory for Earth Surface Processes, College of Urban and  
11 Environmental Sciences, Peking University, Beijing 100871, China

12 <sup>4</sup>State Key Laboratory of Regional and Urban Ecology, Research Center for Eco-Environmental  
13 Sciences, Chinese Academy of Sciences, Beijing 100085, China

14

15 **Corresponding Author:**

16 Yan Li, Ph.D.

17 Institute of Land Surface System and Sustainable Development, Faculty of Geographical Science,  
18 Beijing Normal University, Beijing, 100875, China

19 Email: [yanli.geo@gmail.com](mailto:yanli.geo@gmail.com)

20

21 **Abstract:** Modeling the coupled human–natural systems (CHANS) is vital for  
22 understanding human–natural interactions and achieving regional sustainability,  
23 offering a powerful tool to alleviating human–water conflicts, ensuring food security,  
24 thereby supporting the region’s pathway toward sustainable development. However,  
25 the scarcity of regional-scale CHANS models constrains progress in practical  
26 applications for regional sustainability. The Yellow River basin (YRB) is an ideal region

27 for modeling regional CHANS due to its closely coupled human and natural systems,  
28 which are stressed by water and ecosystem fragility. Here, we developed the CHANS-  
29 SD-YRB model using the System Dynamics approach, integrating 10 sectors essential  
30 for modeling human-water interactions of the basin, including five human sectors  
31 (Population, Economy, Energy, Food, and Water Demand) and five natural sectors  
32 (Water Supply, Sediment, Land, Carbon, and Climate). The model can simulate  
33 evolution and feedbacks of the YRB CHANS annually at provincial and sub-basin  
34 scales, while conserving hydrological connectivity between sub-basins. The model can  
35 accurately reproduce historical CHANS dynamics, achieving strong quantitative  
36 agreement with historical data ( $R > 0.95$  for human sectors and  $R > 0.7$  for natural  
37 sectors), which supports its applicability for scenario analyses and future projections.  
38 We applied the model to explore human–natural system dynamics under a future  
39 baseline scenario, assuming the continuation of existing policies and climate projection  
40 under middle of the road scenario (SSP–RCP 2-4.5). The future projections (2021-2100)  
41 indicate that achieving sustainable development in the YRB will remain challenging,  
42 though economic growth and food security are expected to improve. Emerging issues,  
43 such as ecological–human water trade-offs, labor shortages, reduced sediment load, and  
44 limited carbon absorption capacity, may hinder regional long-term sustainability.

45 **Keywords:** coupled human-natural systems, regional modeling, system dynamics,  
46 the Yellow River Basin

## 47 **1 Introduction**

48 Coupled human and natural systems (CHANS) emphasize the reciprocal feedback  
49 and co-evolution between human and natural systems, offering an integrated framework  
50 for diagnosing complex problems and guiding sustainable development (Fu and Li,  
51 2016). By capturing dynamic interactions of interconnected components, CHANS  
52 theories and models enable more effective policies and interventions that align  
53 ecological integrity with socioeconomic progress (Motesharrei et al., 2016; Verburg et  
54 al., 2016). Numerous integrated modelling approaches have been developed to simulate

55 human–natural interactions at the global scale. These include system dynamics-based  
56 integrated assessment models (IAMs), such as ANEMI (Breach and Simonovic, 2021),  
57 FeliX (Rydzak et al., 2013; Ye et al., 2024), and FRIDA (Rajah et al., 2025), process-  
58 based and optimization-based IAMs (Vaidyanathan, 2021), and Earth system models  
59 with synchronously coupled human components, such as E3SM-GCAM (Di Vittorio et  
60 al., 2025) and integrated Earth system models (iESMs) (Jain et al., 2022). These models  
61 effectively characterize human–natural interactions at the global scale, and have been  
62 applied to assess the impacts of climate change on human society (e.g., agriculture  
63 (Monier et al., 2018), economic damage (Wang et al., 2020b), fatalities increase and  
64 welfare loss (Dottori et al., 2018)), and humans’ feedback on the Earth system, such as  
65 those from climate mitigation on water and food security (Cheng et al., 2022; Fujimori  
66 et al., 2022).

67 Currently, most CHANS models are at the global scale (Calvin and Bond-  
68 Lamberty, 2018) with much fewer regional models. While global modeling research  
69 has deepened our knowledge of dynamic feedbacks among Earth’s spheres and system  
70 evolution under climate change, sustainability challenges often manifest at regional  
71 scales, where social and ecological dynamics are more intricately intertwined (Liu et  
72 al., 2007). Compared to global CHANS, regional CHANS are open systems that  
73 continuously exchange energy and materials with other regions and the global system,  
74 e.g., water resources and electricity transfers (Dobbs et al., 2023; Zhang et al., 2022a)  
75 and trade (Ristaino et al., 2021), resulting in pericoupling and telecoupling of different  
76 systems (Liu, 2017). Besides, regional CHANS are shaped by more immediate and  
77 complex human influences and stressors, such as urban expansion (van Vliet, 2019),  
78 ecological protection (Xu et al., 2017; Yang et al., 2022), and water resource regulation  
79 policies (diversion and allocation) (Song et al., 2024), which alter regional CHANS  
80 dynamics. Due to their diverse ecological and socioeconomic resilience, regional  
81 CHANS exhibit heterogeneous responses to external weather events and climate  
82 change, as evidenced by differing responses in crop yield (Hasegawa et al., 2021) and

83 economic production to extreme heat and warming (Waidelich et al., 2024a).  
84 Furthermore, the coarse spatiotemporal resolution of global models limits their capacity  
85 to support effective decision-making for regional development (X. Li et al., 2018). As  
86 such, advancing regional CHANS modeling is essential for informing adaptive  
87 strategies in the face of growing regional environmental and societal pressures.

88 To address this limitation, many regional CHANS models have been developed at  
89 various regional scales (e.g., national, basin, and urban) using System Dynamics (SD)  
90 and agent-based modeling (ABMs) techniques. Notable examples include the ANIME-  
91 Yangtze model (Jiang et al., 2022), the T21-China (Qu et al., 2020), and the iSDG-  
92 Australia model (Allen et al., 2019), all based on SD, the Jordan Water Model (Yoon et  
93 al., 2021) with its core on ABM, as well as integrated models in the San Juan River  
94 Basin (Hyun et al., 2019) and the Heihe River Basin (Li et al., 2021). These models are  
95 designed to capture finer-scale dynamics and region-specific human–natural  
96 interactions, since they embed localized characteristics (e.g., fishing ban, reservoir  
97 operation strategies, demographic policies, transboundary flows) and account for  
98 heterogeneity overlooked by global models. As a result, regional CHANS models offer  
99 stronger policy relevance, providing actionable insights for national, basin, and urban  
100 decision-making, and advancing CHANS research across multiple scales.

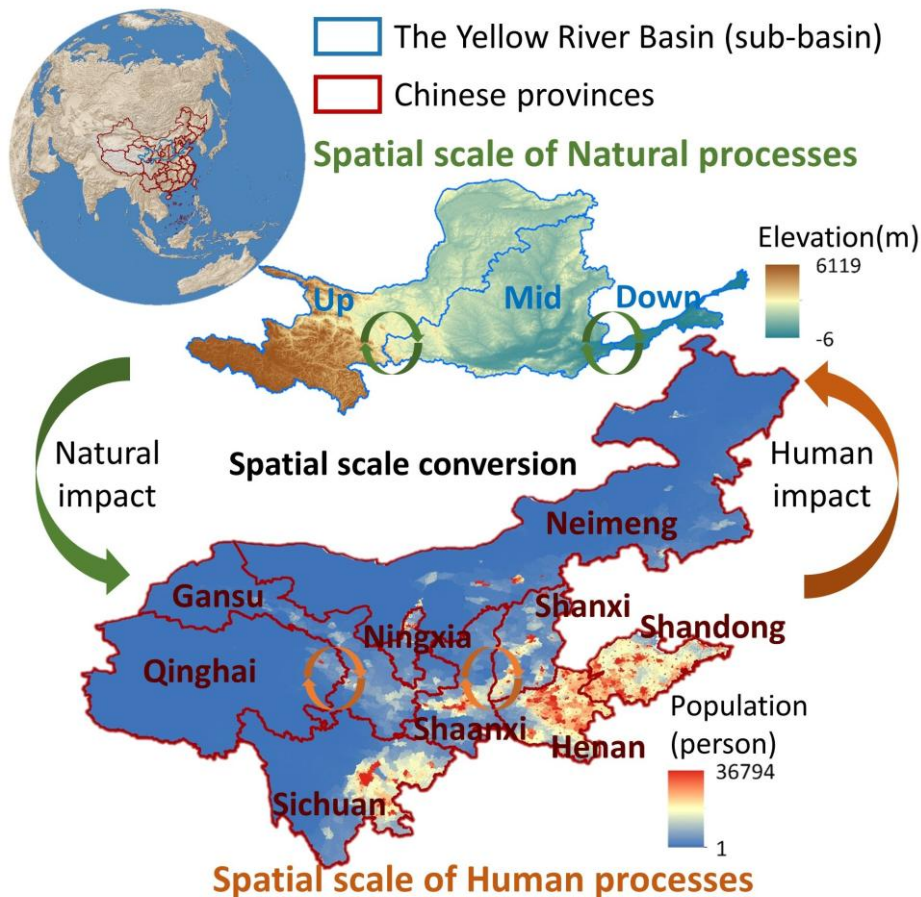
101 The Yellow River Basin (YRB) in China is one of the regions where conflicts  
102 between human and natural systems are most acute and complex, particularly in terms  
103 of human–water relations, due to the severe imbalance between socioeconomic  
104 development and natural hydrological, ecosystem processes. The YRB faces severe  
105 water stress, with the water resource utilization rate exceeding 80% (Feng and Zhu,  
106 2022; Zhang et al., 2022b). Intensive water extraction has triggered a series of  
107 ecological and environmental issues, including flow interruptions, water pollution, and  
108 declining groundwater levels, all of which in turn constrain socioeconomic  
109 development. The Yellow River traverses the Loess Plateau (Zhu et al., 2019), where  
110 severe soil erosion makes the Yellow River one of the most sediment-laden rivers

111 globally (Fu et al., 2011; Yin et al., 2021). The pronounced spatial and temporal  
112 variability in streamflow and sediment load leads to significant riverbed aggradation,  
113 frequent flooding, and disruption of agricultural production and other livelihood  
114 activities (Miao et al., 2016). Due to internal hydrological connectivity, sub-basins are  
115 highly interconnected and are susceptible to upstream influences. Upstream water  
116 overuse diminishes downstream availability (Wei et al., 2023), a factor that played a  
117 major role in flow interruptions during the 1990s (Changming and Shifeng, 2002; Wang  
118 et al., 2019). Ecological challenges differ across the subbasin, with the upstream facing  
119 ecosystem degradation and limited water retention (Ning et al., 2022), the midstream  
120 characterized by soil erosion and large-scale ecological restoration (Fu et al., 2011), and  
121 the downstream focusing on wetland conservation (Fu et al., 2023). Policy measures  
122 aimed at ecological restoration, such as afforestation and cropland conversion, have  
123 increased vegetation cover, reduced sediment loads but also decreased runoff,  
124 exacerbating water scarcity (Feng et al., 2016; Wang et al., 2016). These interlinked  
125 dynamics underscore the YRB as a complex coupled human–natural system, where  
126 addressing environmental challenges requires an integrated, systems-oriented approach.

127       The existing models for the YRB are typically designed for specific problems with  
128 a narrow application focus and only represent a limited set of human and natural  
129 components within the CHANS. These include limited nature-to-human impact  
130 pathways, e.g., low flows threatening farmers’ livelihoods (Liu et al., 2008), the damage  
131 of floods and droughts on agriculture (Zhang et al., 2015), as well as human-to-nature  
132 impact pathways, e.g., effects of ecological restoration policy on hydropower and  
133 water–sediment–carbon dynamics (Wu et al., 2025; Yan et al., 2024), and the impacts  
134 of irrigation water-saving and salinity-control practices on crop yield and water  
135 productivity (Wu et al., 2023). These models focus on isolated components of CHANS,  
136 with limited consideration of fully coupled human–natural interactions, which limits  
137 their capacity to represent full human–natural interactions and support regional  
138 decision-making.

139 To address the gap in CHANS modeling for the YRB, following our previously  
 140 proposed CHANS modeling framework for the basin (Sang et al., 2025b), we  
 141 implemented the framework to develop the coupled human and natural systems model  
 142 for the YRB (CHANS-SD-YRB) using the System Dynamics approach. Through  
 143 dynamic interaction with policies, climate change, human activities, and environmental  
 144 feedbacks, the CHANS-SD-YRB model provides a platform for predicting system  
 145 dynamics, conducting scenario analyses, evaluating policies, and optimizing water-  
 146 food-carbon synergies. This study offers both theoretical and practical insights for  
 147 advancing regional CHANS modeling and promoting sustainable development in the  
 148 YRB.

149 **2 Description of the CHANS-SD-YRB**



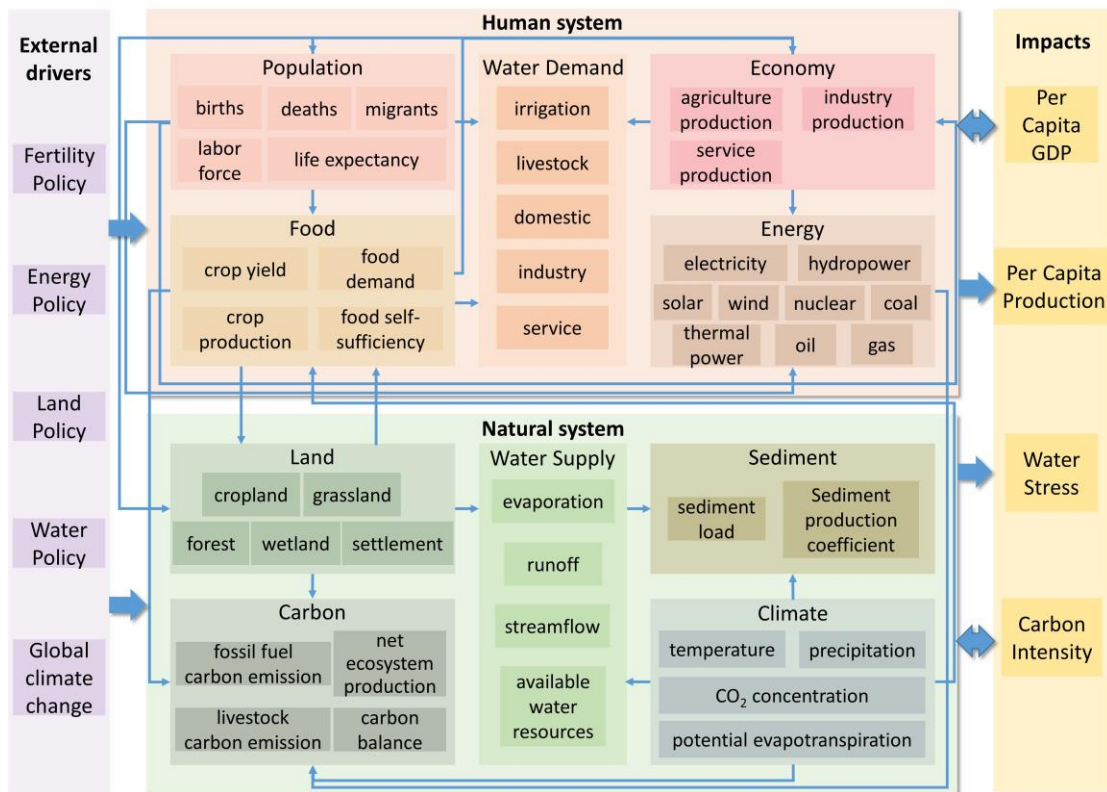
150

151 Fig.1 Geolocation of the Yellow River Basin and boundary of the natural and human  
 152 processes in the CHANS-SD-YRB model. Natural processes are simulated at the sub-

153 basin scale (base map: elevation), and human processes at the provincial scale across  
154 nine provinces (base map: population density in 2020).

155 We developed the CHANS-SD-YRB based on system dynamics, a method well-  
156 suited for capturing complex system behaviors characterized by nonlinearity, multi-  
157 level structures, and feedback loops (Forrester, 1968; Richardson, 2011). The model  
158 was constructed and implemented using the VENSIM DSS (Ventana Systems, 2023)  
159 software platform, operating on an annual time step. The CHANS-SD-YRB simulates  
160 both human and natural processes for historical simulations (1981–2020) and future  
161 projections (2021–2100). Human processes are simulated at the provincial scale,  
162 covering the nine provinces along the Yellow River (Qinghai, Sichuan, Gansu, Ningxia,  
163 Neimeng, Shaanxi, Shanxi, Henan, and Shandong), while natural processes are  
164 simulated at the sub-basin scale (up-, mid-, and downstream) (Fig.1). The model is  
165 designed to capture the various interactions within and between different components  
166 of human system and natural system across administrative and hydrological units. The  
167 spatial scale conversion between provincial and sub-basin levels relies on weights (e.g.,  
168 the proportion of sub-basin-level values to provincial total values) derived from  
169 historical high-resolution gridded datasets of human-related variables. These weights  
170 enable disaggregation of provincial outputs to the sub-basin level (see Supporting  
171 Information S4 for details). Given the availability of gridded data for human processes  
172 and the strong correlations among relevant variables, gridded population and GDP data  
173 were used as proxies to disaggregate demographic variables and economic and human  
174 carbon emissions, respectively, from provincial-level to the sub-basin scale (Table S3).

175 **2.1 Model structure**



176  
 177 Fig.2 Structure of the CHANS-SD-YRB, which shows sectors of human and natural  
 178 systems, their key processes and interactions.

179 Drawing on the modeling framework of CHANS in the YRB (Sang et al., 2025b),  
 180 we designed the CHANS-SD-YRB structure (Fig. 2), including five sectors related to  
 181 human society (*Population, Economy, Energy, Food, and Water Demand*), and five  
 182 sectors related to natural ecosystem (*Water Supply, Sediment, Land, Carbon, and*  
 183 *Climate*).

184 These sectors are interconnected to represent various human-natural interactions  
 185 as summarized below. Key interactions among human system modules are summarized  
 186 below. The *Population* sector affects food demand (*Food*), residential water use (*Water*  
 187 *Demand*), household electricity and gas consumption (*Energy*), and settlement land area  
 188 (*Land*). The sector also interacts dynamically with the *Economy* sector, where economic  
 189 output influences deaths and migrants, while the labor force, in turn, drives economic  
 190 production. The *Economy* sector drives energy uses (electricity, coal, oil, and gas use)

191 from *Energy*, as well as industrial and service water withdrawal from *Water Demand*.  
192 The gross agricultural production in the *Economy* is made up of crop and livestock  
193 production (*Food*). The *Energy* sector produces fossil fuel emissions in the *Carbon*  
194 sector. The *Food* sector is affected by the *Land* and *Climate* sector, and it also  
195 determines irrigation water withdrawal (*Water Demand*) and livestock-related  
196 emissions (*Carbon*). Additionally, the *Food* sector interacts closely with the *Land* sector,  
197 where crop production depends on cropland area, which, in turn, is influenced by food  
198 self-sufficiency. The *Water Demand* sector affects streamflow in the *Water Supply*  
199 sector through consumptive water use.

200 The key interactions among natural system modules are listed below. The *Land*  
201 sector influences evapotranspiration in the *Water Supply* sector through vegetation  
202 coverage, and it influences carbon absorption in *Carbon* sector through land use area.  
203 The carbon absorption is also affected by climatic variables including temperature,  
204 precipitation, and CO<sub>2</sub> concentration. Similarly, runoff in the *Water Supply* sector is  
205 affected by precipitation, precipitation intensity (mm/h, the rate of rainfall within one  
206 hour calculated from daily data), and potential evapotranspiration. Streamflow  
207 influences sediment dynamics in the *Sediment* sector together with the *Climate* sector.

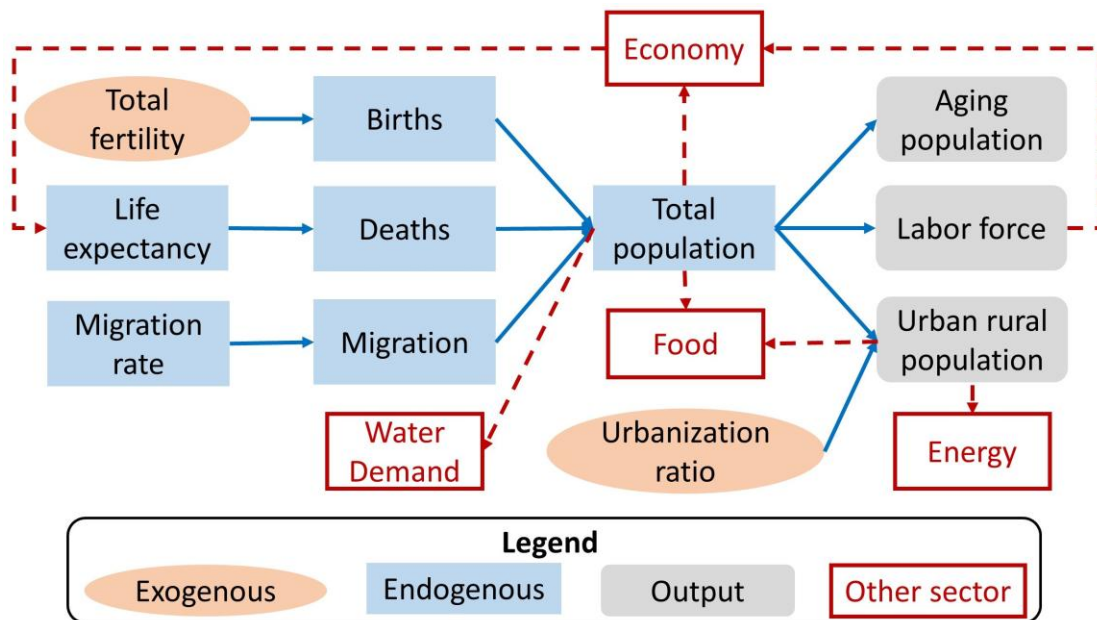
208 In addition, the CHANS dynamics in the YRB are modulated by external drivers,  
209 including policies and global climate change that affect various modeled processes (e.g.,  
210 fertility, energy, land use, and water). With comprehensive representation of CHANS  
211 processes and their interactions, the CHANS-SD-YRB model is capable of generating  
212 integrated indicators to assess the state of the coupled system, such as per capita GDP,  
213 per capita food production, water stress, and carbon intensity. These indicators not only  
214 serve as evaluation metrics but also feed back to influence the internal dynamics of the  
215 human–natural system in the YRB.

## 216 **2.2 Sector description**

217 The CHANS-SD-YRB model focuses on the essential human–natural processes in  
218 the YRB, with a particular emphasis on human–water interactions. To this end, it has a

219 comprehensive representation of the full range of natural and human processes that  
 220 influence water use and supply. Formulation of each sector aims to explicitly account  
 221 for cross-sectoral interactions as fully as possible while remaining sufficiently simple  
 222 to be implemented within the SD software. Considering data availability and the spatial  
 223 scales of process, human sectors (*Population, Economy, Energy, Food, and Water*  
 224 *Demand*) are simulated at the provincial level, while natural sectors (*Water Supply,*  
 225 *Sediment, Land, Carbon, and Climate*) are simulated at the sub-basin level within the  
 226 YRB. Next, we describe each sector and its key formulation and provide full details in  
 227 Supporting Information S2.

228 **2.2.1 Population**



229  
 230 Fig.3 Structure of the *Population* sector. Blue lines indicate connections inside the  
 231 sector, red dotted lines indicate connections with other sectors.

232 Population dynamics are driven by births, deaths, and migration (Fig. 3). Births  
 233 are calculated based on exogenous total fertility rates derived from historical data  
 234 (Equation S2) to reflect the strong influence of China's Family Planning Policy. Deaths  
 235 are determined by the life expectancy, which is modeled as a function of human well-  
 236 being (Equations S3-S6). Migration is calculated based on historical statistical data and  
 237 per capita GDP differences between YRB and the national average level (Equations S7-

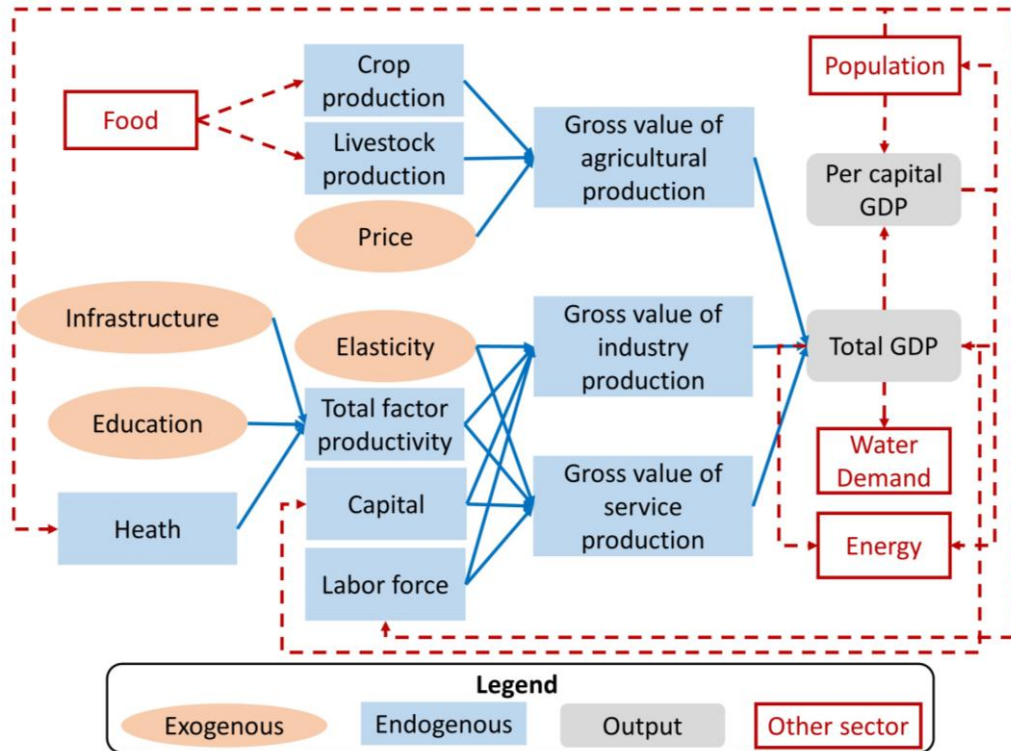
238 S8). The total population is characterized by age and gender with exogenous  
 239 urbanization ratios. The output of *Population* sector drives *Economy*, *Energy*, *Food*,  
 240 and *Water Demand* sectors through labor force, urban and rural populations.

241 The key variable, total population, is modeled using the age-structured  
 242 mathematical method (Kemei et al., 2024), which categorizes individuals by one-year  
 243 age group and gender (Equation 1),

$$244 \text{Pop}_{g,a} = \text{IniPop}_{g,a} + \begin{cases} \int (B_{g,a} + NM_{g,a} - D_{g,a})dt, & a = 0 \\ \int (\text{Pop}_{g,a} + NM_{g,a} - D_{g,a})dt, & 1 \leq a \leq 99, a = 100 \text{ and over} \end{cases} \quad (1)$$

246 where *Pop* is population, subscript *g* and *a* are gender (*g* = M is male, *g* = F is female)  
 247 and age (*a* = 0-100 and over); *IniPop<sub>g,a</sub>* is the population in the initial year, *B<sub>g,a</sub>* is the  
 248 births, *D<sub>g,a</sub>* is the deaths, and *NM<sub>g,a</sub>* is the net migrants (i.e., immigrants – emigrations).

249 **2.2.2 Economy**



250  
 251 Fig.4 Structure of the *Economy* sector. Blue lines indicate connections inside the  
 252 sector, red dotted lines indicate connections with other sectors.

253 The *Economy* sector simulates production activities in agriculture, industry, and

254 services, which in turn drive changes in the *Population, Energy, and Water Demand*  
255 sectors (Fig. 4).

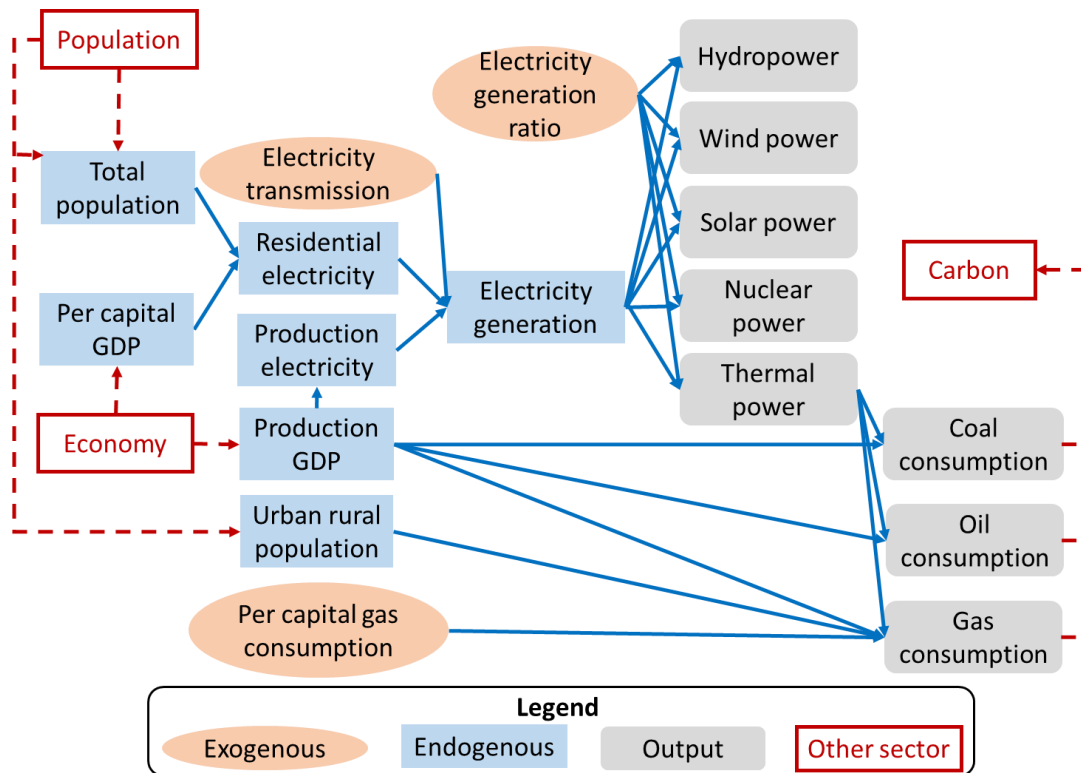
256 The gross product of industry and services is calculated using the Cobb-Douglas  
257 production function (Cobb and Douglas, 1928) to account for multiple factors in the  
258 economy (Equation 2). Exogenous variables (infrastructure, education, and elasticity),  
259 and endogenous variables (health and labor force) from the *Population* sector  
260 (Equations S10-S21) all affect the gross domestic product in industry and service  
261 ( $GDP_s$ ),

$$262 \quad GDP_s = IniGDP_s \times TFP_s \times \left(\frac{L_s}{IniL_s}\right)^{1-\alpha_s} \times \left(\frac{K_s}{IniK_s}\right)^{\alpha_s} \quad (2)$$

263 where subscript  $s$  represents industry and service,  $IniGDP_s$  is the initial GDP;  $TFP_s$  is  
264 the total factor productivity calculated from exogenous (infrastructure, education, and  
265 elasticity) and endogenous variables (health and labor force) (Equations S10-S13);  $L_s$   
266 represents the labor force and  $IniL_s$  is its initial value (from *Population* sector);  $\alpha_s$  and  
267  $1-\alpha_s$  are capital and labor elasticities from T21-China (Qu et al., 2020) and calibrated  
268 using historical data;  $K_s$  and  $IniK_s$  refer to the capital stock and its initial level.

269 Gross agricultural production includes crop and livestock production from *Food*  
270 sector, calculated by their respective prices (Equations S22-S23).

271 **2.2.3 Energy**

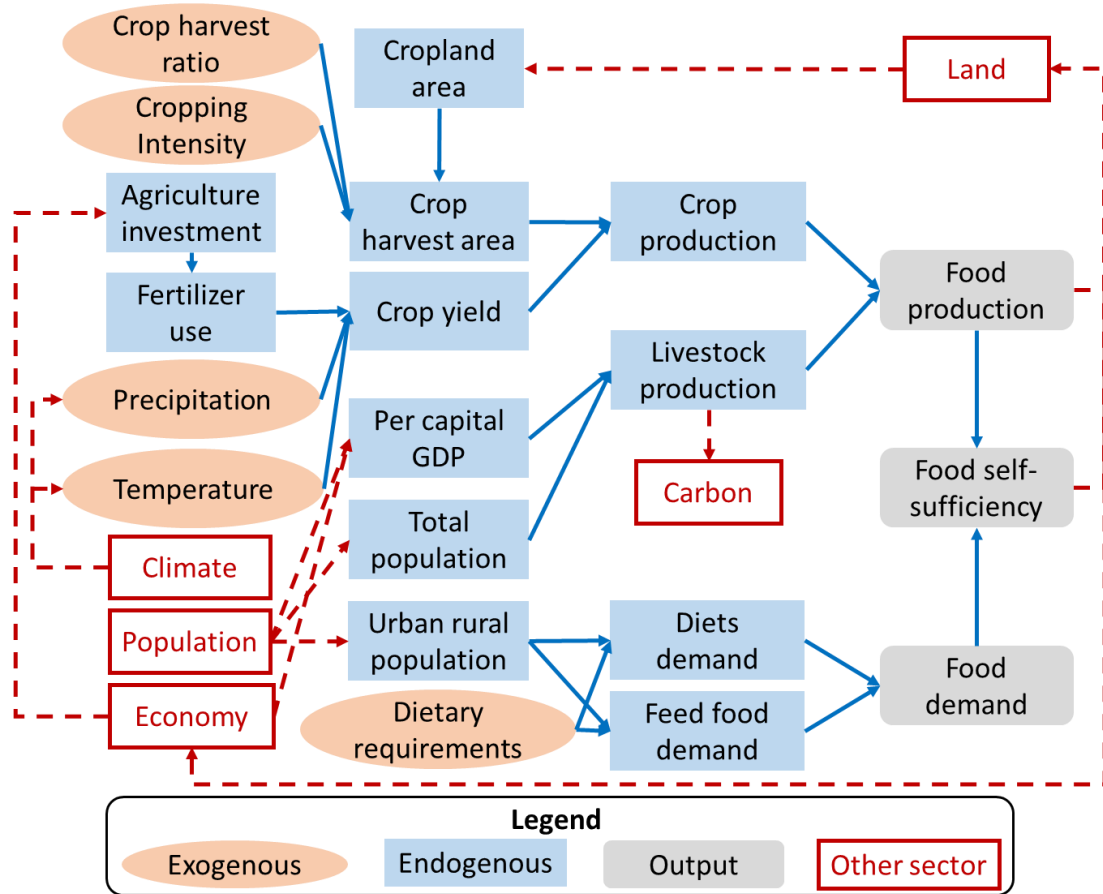


272  
 273 Fig.5 Structure of the *Energy* sector. Blue lines indicate connections inside the sector,  
 274 red dotted lines indicate connections with other sectors.

275 The *Energy* sector simulates production, consumption, and the structure of the  
 276 energy system, encompassing fossil fuels (coal, oil, and gas) and electricity (Fig. 5).  
 277 Energy production and consumption are always balanced in this sector. Electricity  
 278 generation is divided into residential and production uses, the former is estimated from  
 279 the linear fit of historical per capita GDP and residential demand, and the latter is  
 280 calculated using GDP and electricity intensity data from the China Energy Statistical  
 281 Yearbook (NBSC, 2020a) (Equations S24-S25). Cross-provincial electricity  
 282 transmission is also incorporated according to the same yearbook. The shares of  
 283 electricity generated from thermal, hydro, wind, solar, and nuclear sources are  
 284 determined by exogenously specified ratios, as reported in the China Energy Statistical  
 285 Yearbook (NBSC, 2020a). The fossil fuel consumption by economic production of  
 286 industry and service sectors is modeled as a linear function of sectoral GDP based on  
 287 historical data (Equations S26-S28). It combines with fossil fuel consumption for

288 electricity generation and residential gas consumption to drive carbon emissions in the  
 289 *Carbon* sector.

290 **2.2.4 Food**



291  
 292 Fig.6 Structure of the *Food* sector. Blue lines indicate connections inside the sector,  
 293 red dotted lines indicate connections with other sectors.

294 The *Food* sector simulates the production of livestock and crops, and food demand,  
 295 and these productions directly affect gross agricultural production in the *Economy*  
 296 sector (Fig. 6). Livestock production ( $Livestock_{pro}$ ) is calculated by an empirical  
 297 function, driven by economic development and population growth (Equation 3),

298 
$$Livestock_{pro} = Pop \times \left( Para_{GL1} + (Para_{GL2} - Para_{GL1}) \times \frac{PCGDP}{PCGDP + ConstGL} \right) \quad (3)$$

299 where  $Para_{GL1}$ ,  $Para_{GL2}$  and  $ConstGL$  are parameters obtained by fitting the historical  
 300 per capita meat production and per capita GDP ( $PCGDP$ ) data.

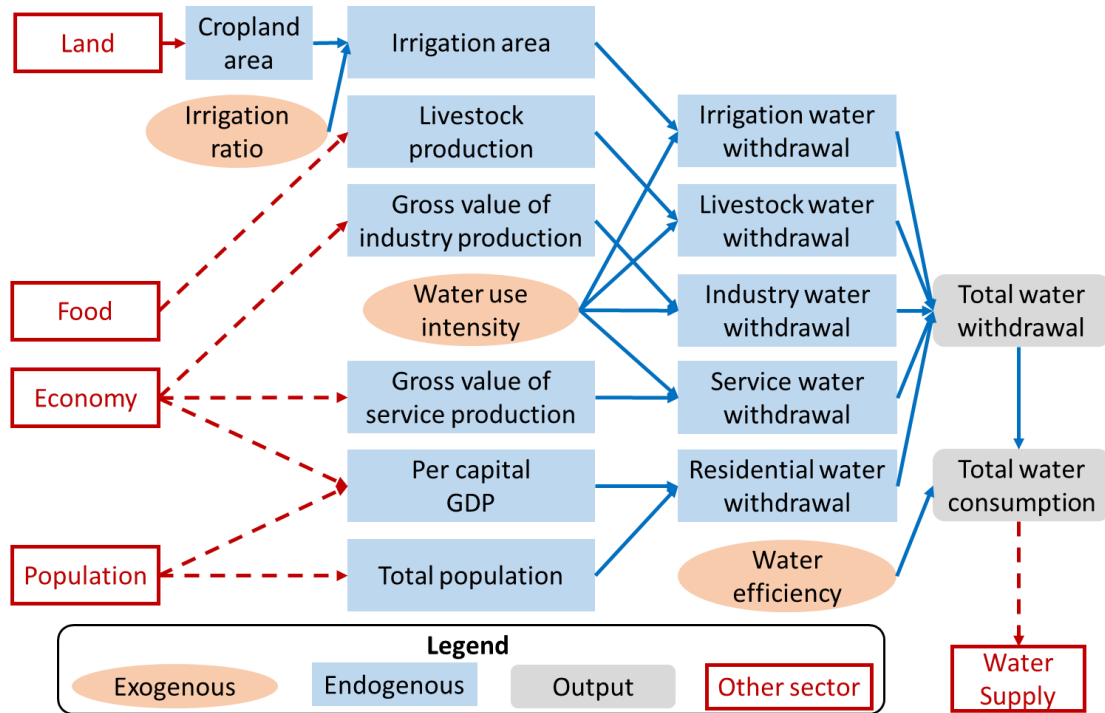
301 Crop production ( $Crop_{pro}$ ) is determined by the yield ( $Yield_c$ ) and harvest area ( $PA_c$ )  
 302 of seven major crop types (subscript  $c$ ): rice, wheat, corn, soybeans, cotton, potatoes,

303 and oil crops (Equation 4). The harvest area is influenced by cropland area from the  
 304 *Land* sector, exogenous cropping intensity and crop harvest ratio. Crop yields are  
 305 positively affected by agricultural investment from the *Economy* sector, along with  
 306 effects of precipitation, temperature, and CO<sub>2</sub> concentration from the *Climate* sector  
 307 (Equations S30-S36).

308 
$$Crop_{pro} = \sum_{c=1}^7 Yield_c \times PA_c \quad (4)$$

309 Food demand encompasses both staple and feed grain demand, which are  
 310 determined by population size from *Population* sector and dietary patterns (Equations  
 311 S37-S41).

312 **2.2.5 Water Demand**



313  
 314 Fig.7 Structure of the *Water Demand* sector. Blue lines indicate connections inside the  
 315 sector, red dotted lines indicate connections with other sectors.

316 The *Water Demand* sector simulates water withdrawal (*WW*) and consumption  
 317 (*WC*) across multiple uses—irrigation, livestock, industry, services, and residential—  
 318 in the nine provinces of the YRB (Fig. 7). Water consumption is derived as the product  
 319 of water withdrawal and water use efficiency reported in the Water Resources Bulletin

320 (YRCCMWR, 2020) (Equations S42-S43), which affects the *Water Supply* sector.

321 Irrigation water withdrawal ( $WW_{irr}$ ) is estimated through a physically-based  
322 function of exogenous irrigation water use intensity ( $WWI_{irr}$ ), cropland irrigation ratios  
323 ( $IR$ ) from the China Agricultural Yearbook (MAARA, 2020), and cropland area  
324 ( $Area_{Cropland}$ ) provided by the *Land* sector (Equation 5).

$$325 \quad WW_{irr} = WWI_{irr} \times Area_{Cropland} \times IR \quad (5)$$

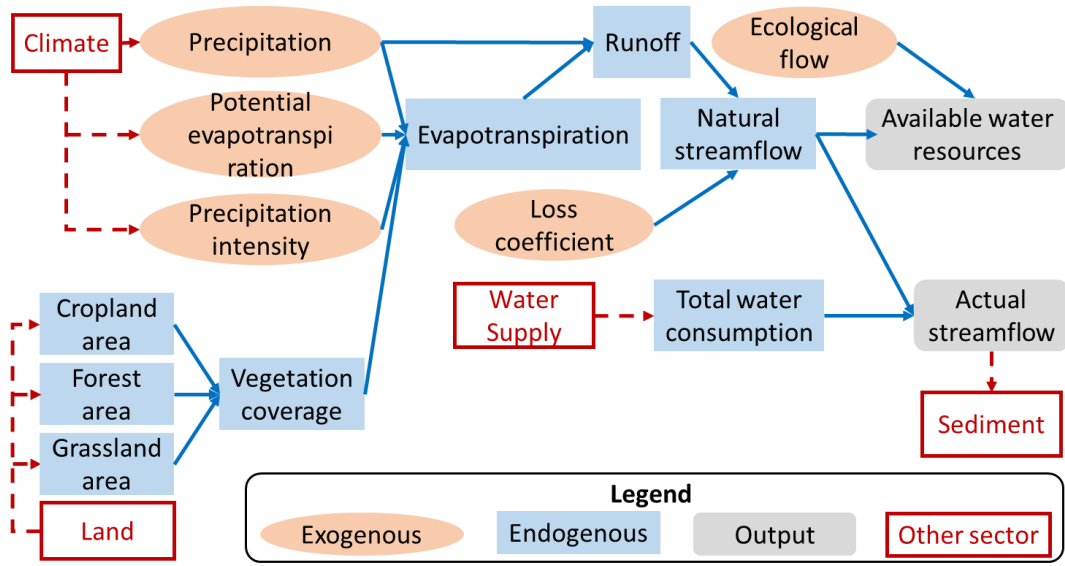
326 The water withdrawal for livestock, industry, and services is also driven by  
327 exogenous sectoral water use intensities collected from the China Statistical Yearbook  
328 and National Long-term Water Use Dataset of China (Zhou et al., 2020), in combination  
329 with livestock production from the *Food* sector, economic output from the *Economy*  
330 sector (Equations S45-S48).

331 Residential water withdrawal ( $WW_{res}$ ) is derived from a non-linear empirical  
332 function of economic development and population growth with an upper limit of per  
333 capita domestic water use (Flörke et al., 2013) because water demand per person cannot  
334 increase indefinitely (Equation 6),

$$335 \quad WW_{res} = Pop \times \left( Para_{GD1} + (Para_{GD2} - Para_{GD1}) \times \frac{PC_{GDP}}{PC_{GDP} + Const_{GD}} \right) \quad (6)$$

336 where  $Para_{GD1}$ ,  $Para_{GD2}$ , and  $Const_{GD}$  are parameters obtained by fitting the historical  
337 per capita domestic water use with per capita GDP ( $PC_{GDP}$ ).

338 **2.2.6 Water Supply**



339

340 Fig.8 Structure of the *Water Supply* sector. Blue lines indicate connections inside the  
341 sector, red dotted lines indicate connections with other sectors.

342 The *Water Supply* sector simulates runoff, discharge, and their changes in each  
343 sub-basin (Fig. 8). Runoff ( $R$ ) is determined by precipitation ( $Pre$ ) and  
344 evapotranspiration ( $ET$ ) based on the water balance principle derived from the Budyko  
345 equation, which is suitable for non-humid regions of China (Yang et al., 2009)  
346 (Equation 7).

347 
$$R = Pre - ET \quad (7)$$

348 The  $ET$  is calculated by various exogenous climate variables from the *Climate*  
349 sector, and vegetation coverage from the *Land* sector (Equations 8-9, S51-S53),

350 
$$ET = \frac{PET \times Pre}{(Pre^n + EP^n)^{\frac{1}{n}}} \quad (8)$$

351 
$$n = Para_{E1} \times \left(\frac{Ks}{PI}\right)^{Para_{E2}} \times FVC^{Para_{E3}} \times e^{Para_{E4} \tan \beta} \quad (9)$$

352 where  $PET$  is potential evapotranspiration at sub-basin, from the *Climate* sector;  $n$  is a  
353 parameter reflecting the basin landscape characteristics, related to saturated hydraulic  
354 conductivity ( $Ks$ ), precipitation intensity ( $PI$ ), average slope ( $\beta$ ), and fraction of  
355 vegetation coverage ( $FVC$ );  $Para_{E1}$ ,  $Para_{E2}$ ,  $Para_{E3}$ , and  $Para_{E4}$  are parameters fitted  
356 from historical data.

357 Runoff and the loss coefficient (defined by the ratio of natural streamflow to runoff)  
 358 determine the natural streamflow due to the water loss during the confluence process  
 359 (Equation S54). Natural streamflow and ecological flow constraints define the upper  
 360 limit of available water resources. By integrating human water consumption from the  
 361 *Water Demand* sector across sub-basins, the model calculates the actual streamflow  
 362 (Equations S55-S57). Actual streamflow is transferred through hydrological  
 363 connectivity from upstream to midstream and then to downstream, ultimately reaching  
 364 the sea, which governs sediment transport processes within the *Sediment* sector.

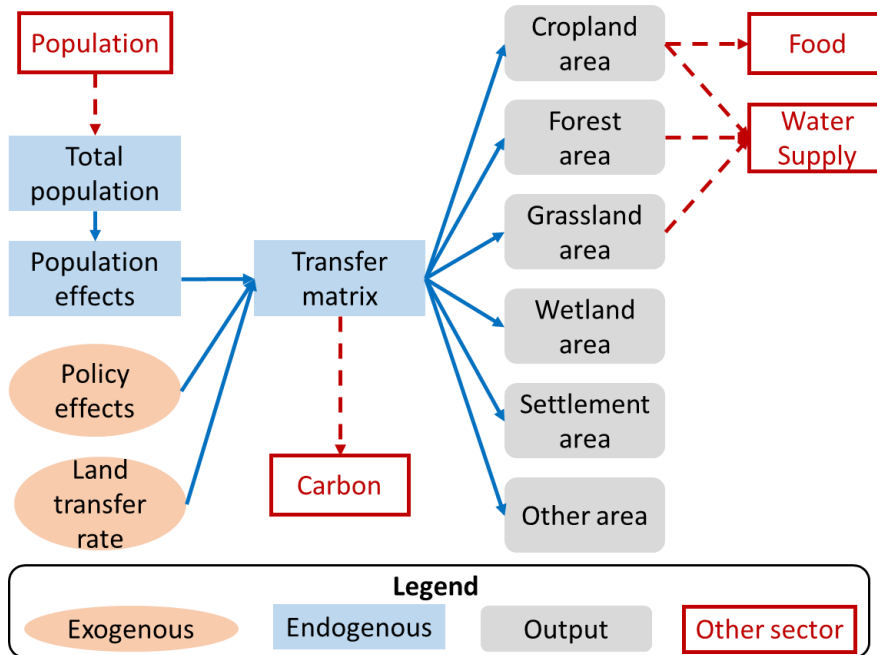
365 **2.2.7 Sediment**

366 The *Sediment* sector estimates sediment load (*Sed*) for each sub-basin using an  
 367 empirical model in the literature (Yin et al., 2023b), which links actual streamflow from  
 368 the *Water Supply* sector to sediment transport,

369 
$$Sed = Para_{SS} \times AS + Const_{SS} \quad (10)$$

370 where *Parass* and *Constss* are derived from linear fitting of historical hydrological  
 371 station data on actual streamflow and sediment load.

372 **2.2.8 Land**



373

374 Fig.9 Structure of the *Land* sector. Blue lines indicate connections inside the sector,

375 red dotted lines indicate connections with other sectors.

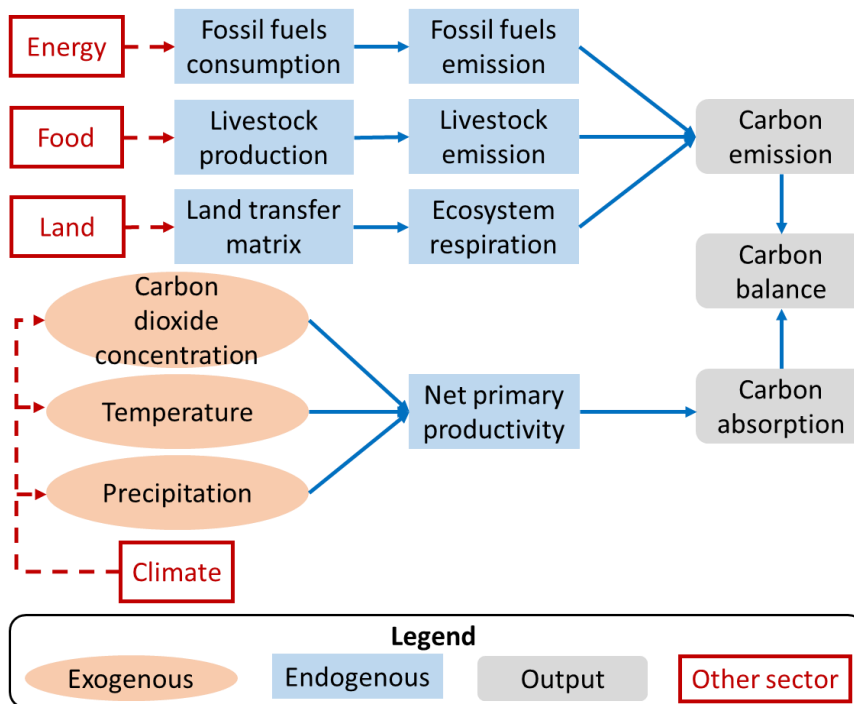
376 The *Land* sector simulates the area changes of six land use types (cropland, forest,  
 377 grassland, wetland, settlement, and others) based on the land transfer matrix obtained  
 378 from historical remote sensing data (Xu et al., 2018). The land transfer matrix calculates  
 379 the inflow and outflow of each land category and can be configured to represent the  
 380 influence of future land use drivers (Fig. 9). This sector outputs vegetation area  
 381 (including forest, grassland, and cropland), which influences the *Water Supply* sector.  
 382 Cropland area changes impact the *Food* sector, while land use conversion also plays a  
 383 role in the *Carbon* sector.

384 Based on the initial land use area ( $IniArea_i$ ), the transfer matrix determines the area  
 385 ( $Area_i$ ) allocated to each land use type (Equations 11, S60-S66),

386 
$$Area_i = IniArea_i + \int (\sum_{i=1}^6 FTM_{i,j} - \sum_{j=1}^6 FTM_{i,j}) dt \quad (11)$$

387 where  $FTM_{i,j}$  is the final land use transfer matrix, indicating the area of land use  $i$   
 388 transferred to land use  $j$ ,  $i$  and  $j$  represent six land use type.

389 **2.2.9 Carbon**



390

391 Fig.10 Structure of the *Carbon* sector. Blue lines indicate connections inside the

392 sector, red dotted lines indicate connections with other sectors.

393 The *Carbon* sector simulates the basin's carbon balance processes, including  
394 carbon emission and absorption, adapted from the carbon cycle of ANEMI (Davies and  
395 Simonovic, 2011). Carbon emissions (*CE*) encompass fossil fuel emissions, and  
396 livestock emission, and ecosystem respiration, which are influenced by outputs from  
397 the *Energy*, *Food*, and *Land* sectors (Fig. 10).

398 Fossil fuel and livestock emissions are calculated based on fossil fuel consumption,  
399 livestock production, and their respective emission coefficients. Ecosystem emissions  
400 include carbon released from burning as well as from the decomposition of biomass,  
401 litter, humus, and charcoal, which are determined by carbon pools' lifespans,  
402 decomposition factor, and respiration coefficients (Equations S67-S93).

403 Carbon absorption (*CA*) is determined by net primary productivity (*NPP*) and land  
404 use area. *NPP* is influenced by climate factors, including CO<sub>2</sub> concentration,  
405 temperature, and precipitation (Equations 12, S63),

$$406 \quad CA = \sum_{i=1}^6 NPP_i \times Area_i \quad (12)$$

407 where *i* represent land use type, land use area (*Area<sub>i</sub>*) from the *Land* sector.

#### 408 **2.2.10 Climate**

409 The *Climate* sector supplies both historical and projected climate data essential for  
410 the *Water Supply*, *Food*, and *Carbon* sectors. The key climate variables comprise  
411 temperature and precipitation (at the sub-basin and provincial levels), as well as  
412 potential evapotranspiration, precipitation intensity, and CO<sub>2</sub> concentration (at the sub-  
413 basin level). These variables are treated as exogenous inputs, without accounting for  
414 potential feedbacks from human activities or natural system responses on regional  
415 climate patterns.

#### 416 **2.3 Data sources**

417 In the model, there are more than 100 exogenous variables, some of which are  
418 initial variables that drive the simulation. These exogenous variables are derived either  
419 from historical statistical data or from fitted results based on historical data (Table S2).

420 All data sources required for the model simulation are listed in Table 1.

421 Table 1. Summary of data sources for the YRB model. Updated from Sang et al.

422 (2025).

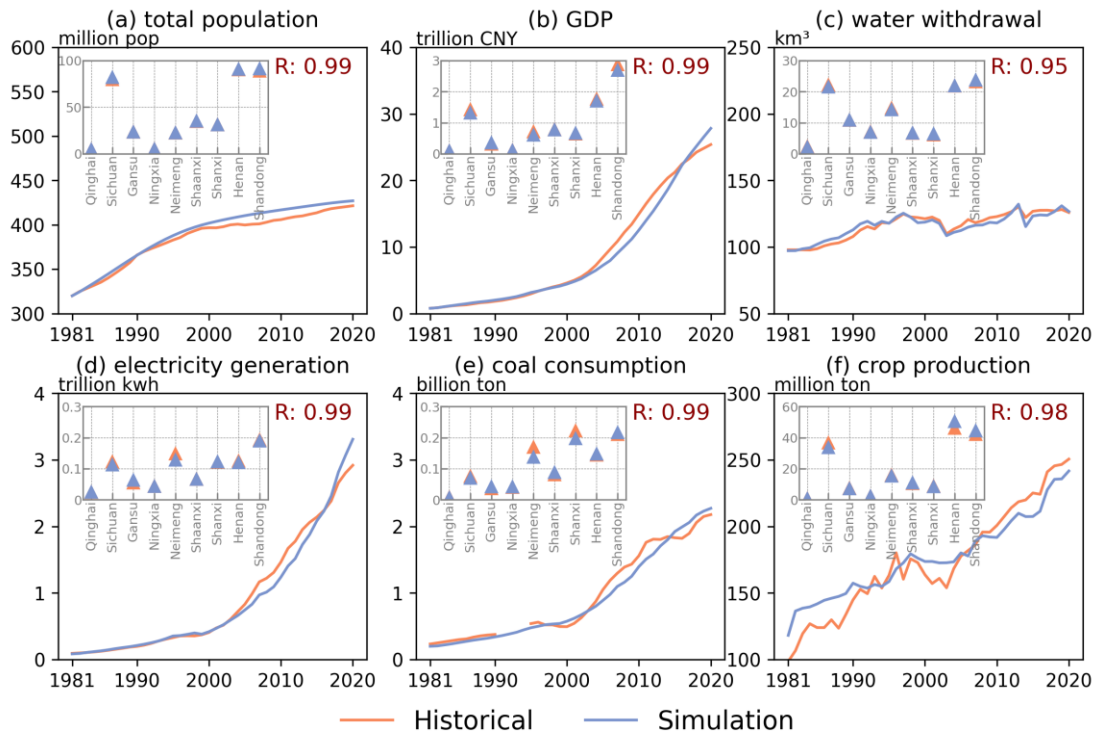
Sector	Variables*	Data sources	Spatial and temporal scale	Time range
<b>Population</b>	age-specific population, births, deaths, migrants	<ul style="list-style-type: none"> <li>China Statistical Yearbook (NBSC, 2020c),</li> <li>China Population Census Yearbook (NBSC, 2020b)</li> </ul>	<ul style="list-style-type: none"> <li>provincial, annual</li> </ul>	<ul style="list-style-type: none"> <li>1981–2023</li> </ul>
<b>Economy</b>	GDP, investment, employment	<ul style="list-style-type: none"> <li>China Agricultural Yearbook (MAARA, 2020),</li> <li>China Statistical Yearbook (NBSC, 2020c)</li> </ul>	<ul style="list-style-type: none"> <li>provincial, annual</li> </ul>	<ul style="list-style-type: none"> <li>1981–2023</li> </ul>
<b>Energy</b>	electricity, coal, oil, gas consumption	<ul style="list-style-type: none"> <li>China Energy Statistical Yearbook (NBSC, 2020a)</li> </ul>	<ul style="list-style-type: none"> <li>provincial, annual</li> </ul>	<ul style="list-style-type: none"> <li>1981–2023</li> </ul>
<b>Food</b>	crop production, fertilizer, irrigated area	<ul style="list-style-type: none"> <li>China Agricultural Yearbook (MAARA, 2020)</li> </ul>	<ul style="list-style-type: none"> <li>provincial, annual</li> </ul>	<ul style="list-style-type: none"> <li>1981–2023</li> </ul>
<b>Water demand</b>	Industrial, domestic, irrigation water withdrawal	<ul style="list-style-type: none"> <li>National Long-term Water Use Dataset of China (NLWUD) (Zhou et al., 2020)</li> <li>China Statistical Yearbook (NBSC, 2020c)</li> </ul>	<ul style="list-style-type: none"> <li>prefectural, annual</li> </ul>	<ul style="list-style-type: none"> <li>1965–2013</li> <li>1981–2023</li> </ul>
<b>Water supply</b>	runoff, streamflow, water stress	<ul style="list-style-type: none"> <li>China Natural Runoff Dataset (CNRD) (Gou et al., 2021),</li> <li>Gauge-based Natural Streamflow Dataset (Miao et al., 2022)</li> <li>Yellow River Water Resources Bulletin (YRCCMWR, 2020)</li> </ul>	<ul style="list-style-type: none"> <li>0.25° grid, Monthly</li> <li>0.25° grid, annual</li> <li>provincial, annual</li> </ul>	<ul style="list-style-type: none"> <li>1961–2018</li> <li>1961–2018</li> <li>1998–2022</li> </ul>
<b>Sediment</b>	sediment load	<ul style="list-style-type: none"> <li>Yellow River Water</li> </ul>	<ul style="list-style-type: none"> <li>provincial,</li> </ul>	<ul style="list-style-type: none"> <li>1998–2022</li> </ul>

		Resources Bulletin (YRCCMWR, 2020)	annual
<b>Land</b>	cropland, forest, grassland, wetland, settlement	<ul style="list-style-type: none"> <li>China land use remote sensing monitoring dataset (CNLUCC) (Xu et al., 2018)</li> <li>Long-term global land surface satellite fractional vegetation cover product (Jia et al., 2015, 2019)</li> </ul>	<ul style="list-style-type: none"> <li>1 km grid, annual</li> <li>1980, 1990, 1995, 2000, 2005, 2010, 2015, 2020</li> </ul>
		<ul style="list-style-type: none"> <li>Carbon Emission Accounts and Datasets (Shan et al., 2018),</li> <li>Global Vegetation Productivity Products (GVPP) (Cui et al., 2016; Wang et al., 2020a; Yu et al., 2018)</li> </ul>	<ul style="list-style-type: none"> <li>Provincial, annual</li> <li>5 km grid, 8 day</li> <li>1997–2021</li> <li>1981–2018</li> </ul>
<b>Climate</b>	temperature, precipitation, CO <sub>2</sub> concentration, potential evapotranspiration and precipitation intensity	<ul style="list-style-type: none"> <li>Gridded daily observation dataset over China region (Wu and Gao, 2013),</li> <li>European Environment Agency (EEA, 2019),</li> <li>China Meteorological Data Service Center (<a href="https://data.cma.cn/">https://data.cma.cn/</a>)</li> </ul>	<ul style="list-style-type: none"> <li>0.25° grid, Annual</li> <li>Global, Annual</li> <li>Meteorological stations, Monthly</li> <li>1961–2020</li> <li>1800-2020</li> <li>1956-2018</li> </ul>

423 \* Listed are some typical variables of each sector

## 424 3 Model validation and application

### 425 3.1 Historical model validation



426

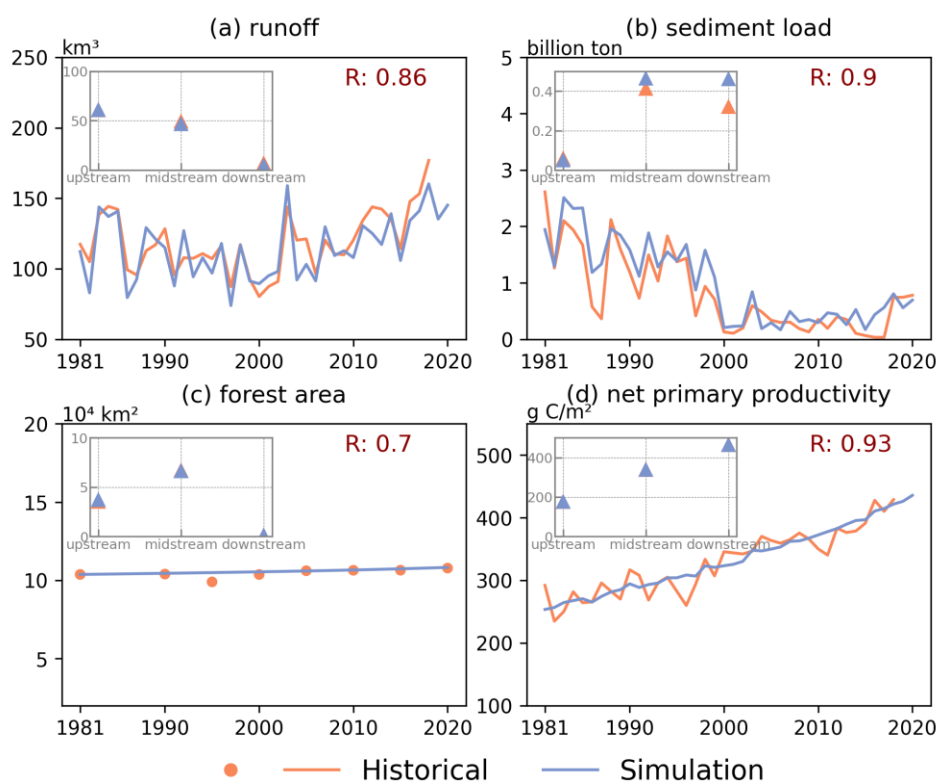
427 Fig.11 Validation of human system processes during historical period of 1981-2020.

428 (a) total population in *Population* sector; (b) GDP in *Economy* sector; (c) water  
429 withdrawal in *Water Demand* sector; (d) electricity generation and (e) coal  
430 consumption in *Energy* sector; (f) crop production in *Food* sector. Pink triangles in the  
431 upper left sub-image represents the average of historical and simulation value in  
432 1981-2020 of each province in the YRB.

433 We compared model performance during the historical period (1981–2020) against  
434 historical data. These data are sourced from multiple channels, including statistical  
435 yearbooks, hydrological stations, remote sensing observations, and outputs from other  
436 models (Table S3).

437 For human sectors, the simulation accuracy of selected key variables from each  
438 sector is consistently high ( $R > 0.95$ ), including total population, gross domestic  
439 product (GDP), water withdrawal, electricity generation, coal consumption, and crop  
440 production across the nine provinces (Fig.11). However, the accuracy varies among

441 provinces, particularly for GDP, electricity generation, coal consumption, and crop  
 442 production. Some provinces, like Neimeng, exhibit lower simulation accuracy for  
 443 certain indicators than others, probably due to the simplification of relevant modelled  
 444 processes, imperfect parameterizations, and external policy interventions. Among all  
 445 sectors, the greatest uncertainty arises in simulating coal consumption, because the  
 446 absence of a clear historical trend results in poor fitting performance. Nevertheless, the  
 447 model performs reasonably well in the human sectors, effectively capturing the  
 448 historical dynamics of human systems in the YRB.



449

450 Fig.12 Validation of the natural system processes during historical period of 1981-  
 451 2020. (a) runoff in *Water Supply* sector; (b) sediment load in *Sediment* sector; (c)  
 452 forest area in *Land* sector, and the historical dataset is discontinuous; (d) net primary  
 453 productivity in *Carbon* sector. Pink triangles in the upper left sub-image represents  
 454 the average of historical and simulation value in 1981-2020 of each sub-basin in the  
 455 YRB.

456 For natural sectors, the simulation accuracy for runoff, sediment load, forest area,

457 and NPP in the YRB is relatively high ( $R > 0.7$ ) (Fig.12). At the sub-basin level, the  
458 overall performance is satisfactory; however, the model shows lower accuracy in  
459 simulating sediment transport in the mid- and downstream. Compared to the human  
460 sectors, the natural sectors generally exhibit lower correlations with historical data,  
461 largely due to the simplifications required when modeling physically complex natural  
462 processes. Nevertheless, the model is still capable of capturing the historical dynamics  
463 of natural processes in the YRB.

464 Sensitivity analyses with randomly generated parameter values reveal growing  
465 uncertainty in the long-term trajectories of socio-economic and natural variables; the  
466 model maintains behavioral robustness across all runs without catastrophic collapse or  
467 unrealistic oscillations (see Supporting Information S3 for details).

## 468 **3.2 Model application for future projection**

### 469 **3.2.1 Future baseline scenario**

470 The future baseline scenario represents a trajectory in which existing plans and  
471 policies continue to operate without substantial changes in external environments. The  
472 development of the baseline scenario primarily relies on variables from the *Population*,  
473 *Economy*, *Water Demand*, and *Land* sector based on available government planning  
474 documents, historical trends, and other projections (Table 2). For future projections,  
475 variables or parameters not specified in the table are held constant at historical levels  
476 from their most recent year. Future climate data (2015-2100) are from the ensemble  
477 mean of 11 CMIP6 models (ACCESS-CM2, CESM2, CMCC-ESM2, GFDL-ESM4,  
478 INM-CM4-8, INM-CM5-0, IPSL-CM6A-LR, MIROC6, MRI-ESM2-0, UKESM1-0-  
479 LL, and HadGEM-GC31-LL) (available at  
480 <https://cds.climate.copernicus.eu/datasets/projections-cmip6?tab=download>) for the  
481 SSP 2-4.5 because this scenario aligns more closely with the climate trends in the YRB.  
482 To ensure temporal consistency, CMIP6 historical climate data (1981–2014) were used  
483 instead of observed historical records. To reduce systemic biases in the raw CMIP6 data,  
484 we applied bias correction using CN05 and ground weather stations observations from

485 1981 to 2014. By statistically aligning the mean of the CMIP6 data with observation  
 486 records, systemic bias is removed while retaining the temporal consistency required for  
 487 long-term simulation.

488 We run the model under the future baseline scenario to project the evolution of  
 489 CHANS in the basin from 2021 to 2100 (see Supporting Information S6 for details of  
 490 future scenario design and supplementary spreadsheet for exogenous variables).

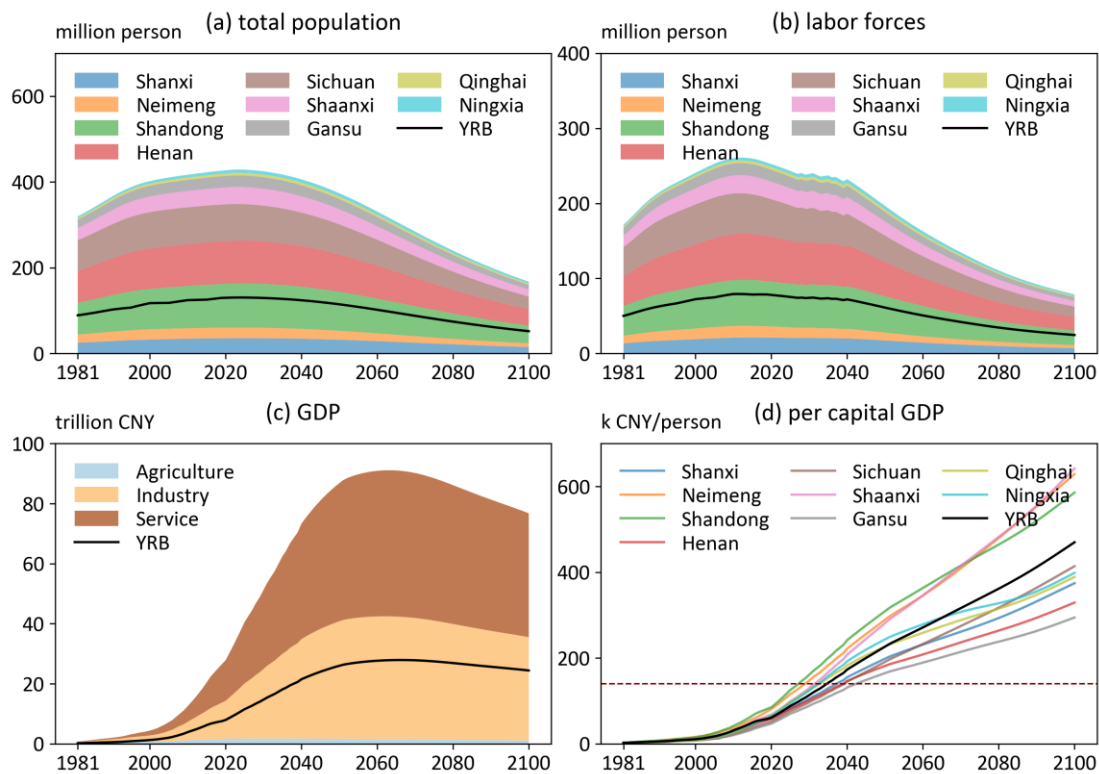
491 Table 2 Settings of key variables in the future baseline scenario

<b>Sector</b>	<b>Variables</b>	<b>Future baseline</b>
<b>Population</b>	• Total fertility	• 2024 United Nations Population Projections
	• Gender ratio	• 2024 United Nations Population Projections
	• Average years of schooling	• The national maximum in 2023 (Germany) as the upper limit
	• Urban and rural population ratio	• Analysis and Forecast of Urbanization Trends in China's Modernization by 2020
	• Labor force	• Delay retirement age
<b>Energy</b>	• Electricity generation sources ratio	• Projected provincial-level energy structure meeting China's carbon peaking and carbon neutrality goals (Li et al., 2024)
	• Irrigation intensity	• Irrigation water use intensity declines linearly (1%/yr) to its minimum value.
<b>Water Demand</b>	• Industry, service, livestock water use intensity	• Industry, service and livestock water use intensity declines linearly (1%/yr) to its minimum value.
<b>Land</b>	• Land use area	• Cropland, forest, and grassland are allowed to be converted into each other, but not to unused land; unused land can be converted to the rest land; wetlands are fixed.
		• Minimum cropland area above the red line

for cropland protection.

- Climate
- Temperature
  - Precipitation
  - Potential evapotranspiration
  - Precipitation intensity
  - CO<sub>2</sub> concentration,
- SSP 2-4.5 — CMIP 6

### 492 3.2.2 Projection of CHANS dynamics in future baseline scenario

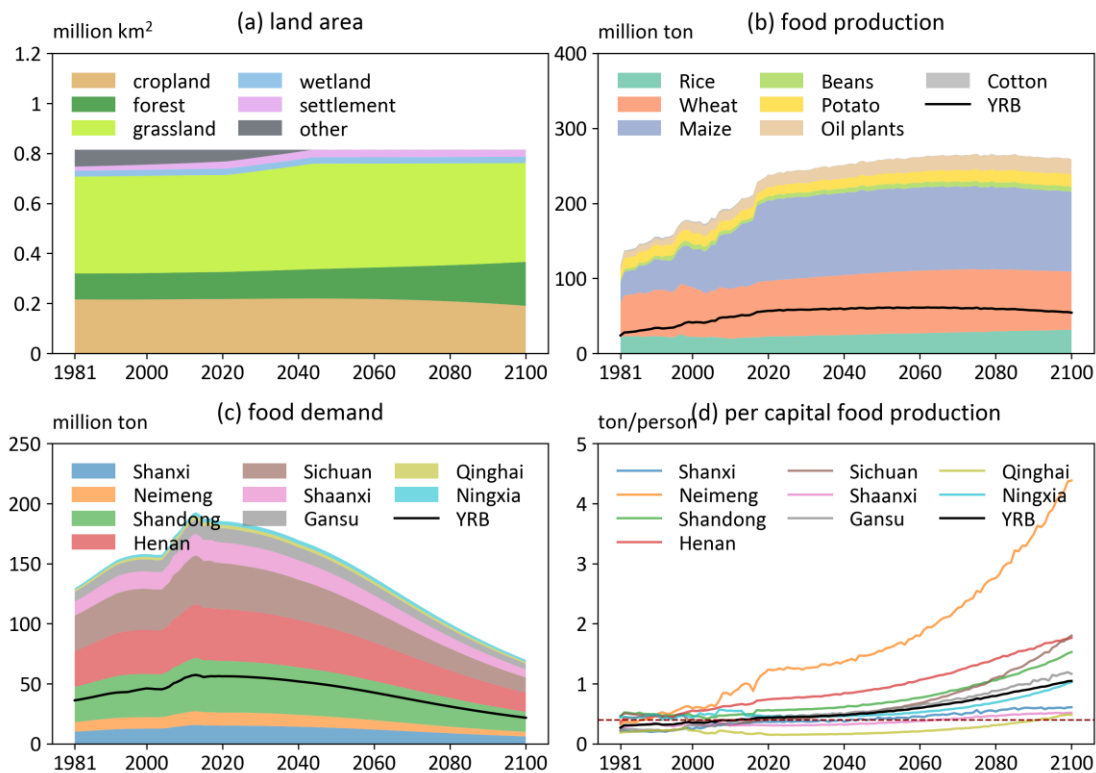


493

494 Fig.13 Changes in key variables of the *Population* and *Economy* sector in the future  
495 baseline scenario: (a) the total population, (b) the total labor forces, (c) the gross  
496 output of agriculture, industry, and service, and the total gross domestic output, (d) the  
497 per capita GDP in nine provinces and YRB.

498 The model simulates human and natural system dynamics under the future  
499 baseline scenario and produces outputs for nine provinces and their corresponding areas  
500 within the YRB. The simulation results are reported either at the provincial level (nine

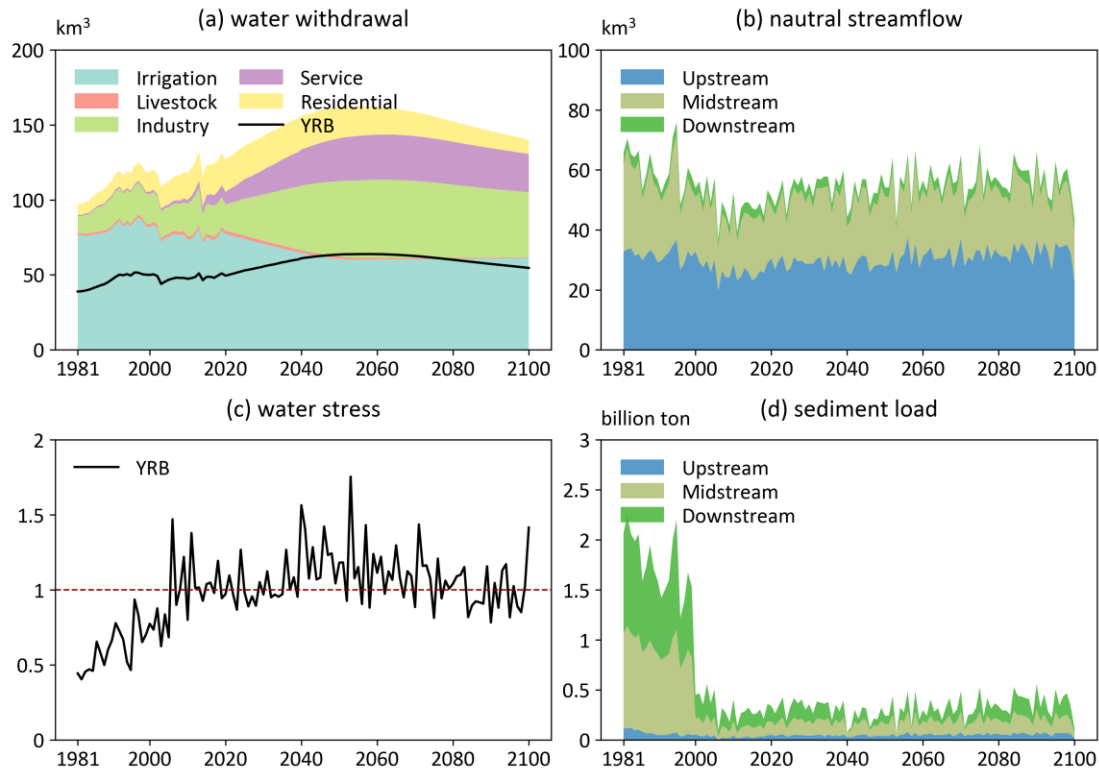
501 provinces) for human system sectors or at the basin level (basin boundary) for natural  
 502 system sectors. The total population in the nine provinces and the YRB is projected to  
 503 peak in 2023 and 2024, at 429 million and 131 million, respectively, driven by declining  
 504 fertility rates (Fig.13 (a)). The labor force peaks earlier, reaching 261 million in the nine  
 505 provinces in 2012 and 79 million in the YRB in 2011 (Fig.13 (b)). After 2025, the labor  
 506 force is projected to increase again due to the delayed retirement policy. GDP in the  
 507 nine provinces is expected to increase until a peak in 2063, at 91 trillion CNY (three  
 508 times the 2020 level, in 2020 constant prices), under the influence of a labor force  
 509 decline, with the YRB reaching its peak four years later (Fig.13 (c)). In contrast to total  
 510 GDP, per capita GDP in all regions is projected to continue rising throughout the future  
 511 period (Fig.13 (d)). Although all provinces demonstrate improvements in economic  
 512 status and living standards, considerable regional disparities persist. Among the nine  
 513 provinces, Shaanxi demonstrates the largest growth in average per capita GDP from  
 514 2021 to 2100 relative to the historical period (1981-2020), with a more than  
 515 seventeenfold increase, while the YRB as a whole shows an over thirteenfold increase.



516

517 Fig.14 Land and food in the future baseline scenario. (a) land area in the YRB; (b-d)  
518 food production of seven crop types, food demand and per capita food production in  
519 nine provinces and the YRB, red dotted line represents the 0.4 tons international food  
520 security threshold.

521 Under the future baseline scenario, land use patterns remain relatively stable based  
522 on historical trends, as no new land policies are introduced and cropland area has to  
523 stay above the red line (a mandatory minimum cropland area for each province for food  
524 security) (Fig.14 (a)). The forest area is projected to increase gradually, reaching 62%  
525 above the 2021 level by 2100, while the cropland area is expected continue declining,  
526 falling 12% below the 2021 level. Total crop production in nine provinces and YRB is  
527 projected to peak in 2079 and 2062 (Fig.14 (b)), respectively, driven by the combined  
528 effects of declining cropland area and increasing crop yields. Food demand in both the  
529 nine provinces and the YRB as a whole peaked in 2013 (193 million tons and 57 million  
530 tons, respectively) (Fig.14 (c)), largely driven by population dynamics. In the future,  
531 per capita food production in the YRB is projected to consistently exceed the  
532 international food security threshold of 0.4 tons per person (Fig.14 (d)). However, in  
533 certain years, provinces such as Qinghai and Shaanxi could fall below this standard.

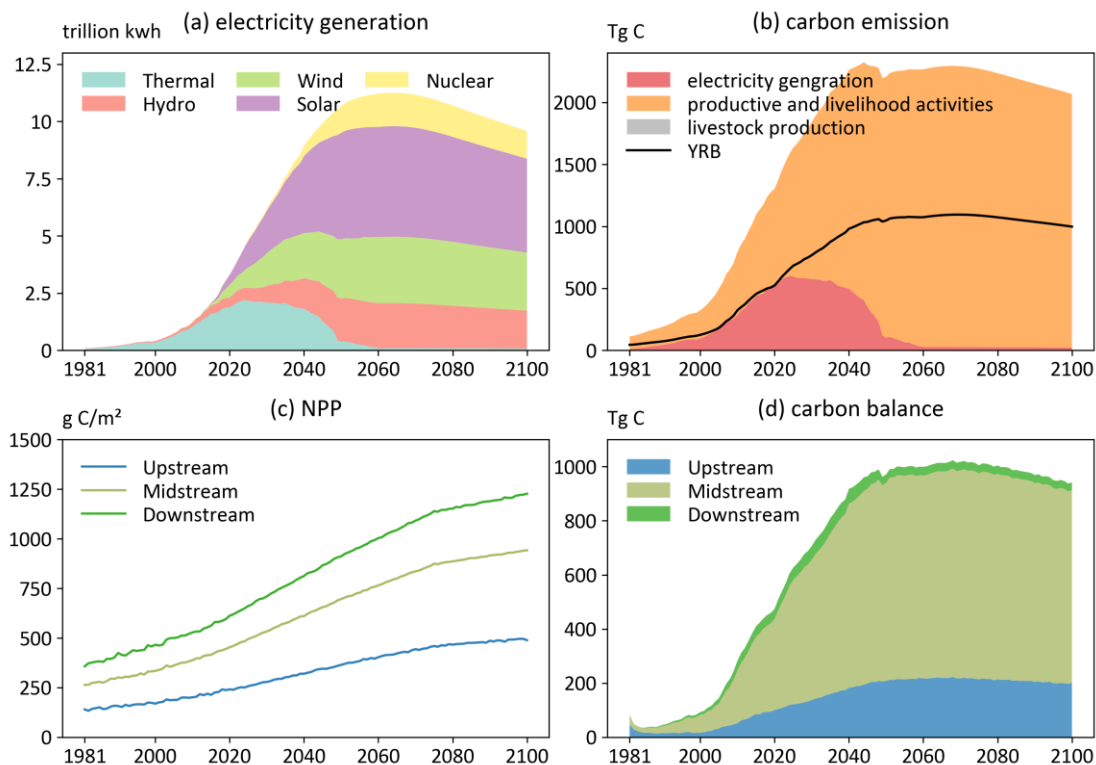


534

535 Fig.15 Water demand and supply in the future baseline scenario. (a) water withdrawal  
 536 across five water-use sectors in nine provinces and the YRB; (b) natural streamflow in  
 537 up-, mid- and downstream; (c) water stress in the YRB, red dotted line represents the  
 538 water security threshold; (d) sediment load in the up-, mid- and downstream.

539 Total water withdrawal in the nine provinces and the YRB is projected to peak in  
 540 2056 and 2058, reaching 162 km<sup>3</sup> and 64 km<sup>3</sup>, respectively (Fig.15 (a)). Irrigation water  
 541 withdrawal is expected to decline, driven by reductions in cropland area and irrigation  
 542 intensity, the latter resulting from improvements in irrigation efficiency assumed in the  
 543 scenario. Peaks in residential, industrial, service, and livestock water withdrawals are  
 544 primarily associated with projected peaks in population and GDP. Natural streamflow  
 545 is projected to exhibit a fluctuating upward trend of 0.073 km<sup>3</sup>/year basin-wide (Fig.  
 546 15(b)), with the most significant growth in the upstream region (0.068 km<sup>3</sup>/year).  
 547 Considering the ecological flow requirement of 18.7 km<sup>3</sup> (YRCCMWR, 2015), water  
 548 stress (calculated as water consumption divided by (natural discharge - ecological flow))  
 549 is expected to decline in the latter half of the century, largely due to the peak and

550 subsequent reduction in water withdrawal. However, overall water stress is projected  
 551 to exceed historical levels in 2041 and will fall below 1 in 38% of the years (Fig.15 (c)),  
 552 reflecting persistent human–water tensions and future trade-offs between ecological  
 553 and human water use. As a result of reduced actual streamflow, sediment transport in  
 554 the Yellow River is projected to decline sharply (Fig.15 (d)), with a 71% decrease in  
 555 sediment load relative to the historical period.



556  
 557 Fig.16 Electricity and carbon in the future baseline scenario. (a) the electricity  
 558 generation from five sources in nine provinces; (b) carbon emission from three  
 559 sources in nine provinces and the YRB; (c-d) the net primary productivity and carbon  
 560 balance in the up-, mid-, and downstream.

561 Since the energy system is transitioning to carbon neutrality goals under the future  
 562 baseline scenario, thermal power generation is projected to decline sharply, while clean  
 563 energy (hydropower, wind, solar, and nuclear) will become the dominant source for  
 564 electricity generation (Fig.16 (a)). The large-scale adoption of clean energy will lead to  
 565 a peak in carbon emissions from electricity generation in 2024 (Fig.16 (b)). In contrast,  
 566 emissions from productive and livelihood activities are projected to rise substantially

567 over time, with total human emissions in the YRB reaching a peak in 2044. NPP is  
568 anticipated to increase markedly in response to CO<sub>2</sub> concentration increase (Fig.16 (c)).  
569 Although the carbon balance of the YRB has remained positive (net carbon source), it  
570 is expected to gradually decline after 2068 (Fig.16 (d)), indicating that the basin's  
571 ecosystems alone cannot fully offset human-induced carbon emissions.

572 The above projections of future baseline scenarios highlight persistent challenges  
573 to achieving sustainable development in the YRB, underscoring the need for integrated  
574 policy responses to address these challenges. Priority should be given to enhancing  
575 water-use efficiency and establishing adaptive water resource allocation mechanisms  
576 that balance ecological and human water needs. Sediment management strategies,  
577 which combine ecological restoration with hydraulic regulation, are necessary to  
578 maintain river stability and delta health. To counter the decline in labor force, policies  
579 should promote industrial upgrading and technological innovation. Strengthening the  
580 basin's carbon mitigation capacity requires accelerating the clean energy transition and  
581 expanding ecological restoration to enhance carbon sequestration. Finally, a multi-  
582 sectoral, CHANS-based governance framework should be established to coordinate  
583 water, land, energy, and carbon management, enabling evidence-based scenario  
584 analysis and adaptive policy design for long-term sustainability.

#### 585 **4 Discussion and conclusions**

586 The development of the CHANS-SD-YRB model involves a series of key  
587 considerations in translating a conceptual framework into a functioning model. The  
588 framework focuses on human–water interactions in the YRB, integrating bidirectional  
589 feedback between human and natural processes. SD was chosen to implement the  
590 framework, as it effectively captures feedback, non-linear relationships, and cross-  
591 sectoral linkages within complex human–natural systems, while remaining practical  
592 and straightforward to use. For quantitative representation of human–natural processes,  
593 we prefer theoretical methods that incorporate key interactions within the system  
594 suitable for implementation using SD. For example, the Budyko framework connects

595 the *Land, Climate, Water Demand*, and *Water Supply* sectors. Relative to distributed  
596 hydrological models, it offers lower computational complexity and reduced data  
597 requirements. The Cobb–Douglas production function links the *Population* and  
598 *Economy* sectors. Compared with Computable General Equilibrium models (Fujimori  
599 et al., 2014a), it is simpler to construct and requires fewer parameters and data inputs.  
600 When no suitable theoretical framework/method is available to describe a process, we  
601 rely on empirical relationships derived from historical data. For example, crop yields  
602 are estimated using fitted relationships between climate variables, fertilizer application,  
603 and historical yields. For processes that cannot be represented through empirical  
604 functions, we apply literature-based estimates to obtain approximate quantitative  
605 relationships, such as fossil fuel emission factors. For processes influenced by external  
606 drivers that cannot be endogenously expressed within the model, we quantify them  
607 using exogenous parameters derived from historical statistics, such as water intensity.  
608 Given the heterogeneous human–natural interactions in the YRB, we represent all  
609 processes at the provincial and sub-basin scales using scale-specific parameters, except  
610 where parameters or data at these levels are unavailable.

611 The CHANS-SD-YRB model explicitly couples multiple human and natural  
612 sectors, enabling a more integrated representation of feedbacks across population,  
613 economy, energy, food, water, sediment, land, carbon, and climate. Unlike models that  
614 focus on specific sectors or isolated subsystems—such as eco-hydrological models and  
615 sediment transport models, which may well capture individual processes but cannot  
616 represent the complex human–nature interactions driving system dynamics. Our  
617 model’s integration of human and natural sectors provides a robust framework for  
618 addressing regional CHANS challenges and offers practical guidance for sustainable  
619 development. The CHANS-SD-YRB model serves as a comprehensive platform for  
620 conducting system dynamics prediction, scenario analysis, policy evaluation, and  
621 optimization, to alleviate human–water conflicts, ensure food security, and achieve  
622 long-term sustainability. For example, analysis of the impacts of the 1987 Yellow River

623 water allocation policy (Song et al., 2024) offer valuable insights for adjusting  
624 interprovincial water distribution to promote sustainable water governance; assessment  
625 of ecological restoration policies (Li et al., 2015) can guide future ecological  
626 engineering; spatiotemporal dynamics of future water gaps can serve as a valuable  
627 reference for planning inter-basin water transfers. The model's flexibility also allows  
628 for the incorporation of additional feedback, for example, linking water scarcity to  
629 industrial output or climate warming to agricultural productivity. These could include  
630 the effects of global warming on human health (Yin et al., 2023a) and economic  
631 activities (Nordhaus, 2017), water constraints on production, dietary shifts influencing  
632 carbon emissions and land use (Ren et al., 2023), and the trade-offs between carbon  
633 mitigation and food security (Xu et al., 2022).

634 Nevertheless, the model remains subject to further refinement. The current  
635 simplifications of natural processes could be replaced with more sophisticated models  
636 to enhance simulation accuracy. For instance, the YRB hydrological processes involve  
637 highly complex human interventions, including reservoir, conservation, and  
638 revegetation projects (Wang et al., 2025). The refined runoff simulations by distributed  
639 hydrological models improve water supply assessments through their better  
640 characterization of spatial heterogeneity in soil, precipitation, and snowmelt (Cong et  
641 al., 2009). For human processes, the *Energy* and *Economy* sectors could be refined to  
642 model more detailed industry subsectors and emerging trends in energy demand driven  
643 by electrification. Moreover, there are still important feedbacks absent from the current  
644 coupling framework. Notable examples include the effects of land use change on  
645 climate, the effects of climate change on economic growth, and the effects of pricing  
646 on energy use and carbon emissions. These missing feedbacks could be incorporated  
647 based on recent studies, including the land use feedback on precipitation through  
648 moisture recycling (Sang et al., 2025a), socioeconomic losses from impacts of climate  
649 change and extremes (Waidelich et al., 2024b), and integration with Computable  
650 General Equilibrium (CGE) models (Fujimori et al., 2014b). Additionally, the model's

651 spatial and temporal resolutions are relatively coarse due to the inherent mismatch in  
652 spatiotemporal scales between human and natural processes. The scale at which we  
653 make the model represents a practical compromise, constrained by data availability and  
654 aligned with the study's objectives. Simulations at finer scales (e.g., monthly, daily, or  
655 gridded) would enhance the representation of natural processes (e.g., hydrological  
656 processes, land use changes, and food production) and the associated spatiotemporal  
657 heterogeneity (e.g., daily simulations can assess the impacts of extreme weather).  
658 However, it may also exacerbate the scale mismatch with socioeconomic processes,  
659 making it challenging to analyze cross-sectoral dynamics. Technically, the inherent  
660 limitations of the SD software restrict the model's ability to represent temporal  
661 fluctuations and spatial variations. To overcome this, transitioning from the VENSIM  
662 platform to a code-based implementation will be necessary, which would also facilitate  
663 coupling with other models. Future research should prioritize these improvements to  
664 strengthen both the performance and applicability of the model.

665 Drawing on the conceptual framework of Sang et al. (2025), this study implements  
666 it into a fully functional, validated System Dynamics model tool, CHANS-SD-YRB 1.0.  
667 The model fills the gap in CHANS modeling for the YRB. It integrates the dynamics  
668 of ten interconnected sectors: *Population, Economy, Energy, Food, Water Demand,*  
669 *Water Supply, Sand, Land, Carbon, and Climate*, achieving reciprocal feedback  
670 between human and natural systems. This model can serve as a robust tool to inform  
671 policy decisions that influence the evolution of coupled human–natural systems and to  
672 explore pathways for optimizing these systems toward sustainability. Furthermore, the  
673 modeling process provides valuable experience for regional CHANS modeling and  
674 contributes to advancing the broader development of CHANS models at the regional  
675 scale.

## 676 **Code and data availability**

677 The CHANS-SD-YRB V1.0 model (Vensim DSS format), along with the input  
678 data and simulation outputs used in this study, are openly accessible at

679 <https://doi.org/10.5281/zenodo.17568963> (Sang, 2025), and  
680 [https://github.com/sangshan-ss/CHANS\\_SD\\_YRB](https://github.com/sangshan-ss/CHANS_SD_YRB).

### 681 **Author contributions**

682 Conceptualization: YL, SS<sup>1</sup>, BF. Data curation: SS<sup>1</sup>. Formal analysis: SS<sup>1</sup>.  
683 Funding acquisition: BF, YL. Investigation: YL, SS<sup>1</sup>. Methodology: SS<sup>1</sup>, YL, BF.  
684 Project administration: YL. Resources: YL. Software: SS<sup>1</sup>, SZ, LY. Supervision: YL,  
685 BF. Validation: SS<sup>1</sup>, SZ, LY. Visualization: SS<sup>1</sup>. Writing – original draft: SS<sup>1</sup>. Writing –  
686 review and editing: SS<sup>1</sup>, YL, SW, YXL, XTW, SS<sup>2</sup>, WZ, XHW. (Note: SS<sup>1</sup> refers to  
687 Shan Sang, and SS<sup>2</sup> refers to Shuang Song, to distinguish between authors with identical  
688 initials.)

### 689 **Competing interests**

690 The authors declare that they have no conflict of interest.

### 691 **Acknowledgements**

692 We thank Dr. Weishuang Qu for developing the Threshold 21 model in the  
693 Millennium Institute that inspired this study, and also for his and Dr. Haiyan Jiang's  
694 generous help with the CHANS-SD-YRB modeling. We also thank the data support  
695 from Dr. Xianghui Kong, and National Earth System Science Data Center, National  
696 Science & Technology Infrastructure of China (<http://www.geodata.cn>).

### 697 **Financial support**

698 This study is supported by the National Natural Science Foundation of China  
699 (Grant No. 42041007), and the Fundamental Research Funds for the Central  
700 Universities.

### 701 **References:**

702 Allen, C., Metternicht, G., Wiedmann, T., and Pedercini, M.: Greater gains for Australia  
703 by tackling all SDGs but the last steps will be the most challenging, *Nat Sustain*, 2,  
704 1041–1050, <https://doi.org/10.1038/s41893-019-0409-9>, 2019.

705 Breach, P. A. and Simonovic, S. P.: ANEMI3: An updated tool for global change  
706 analysis, *PLoS ONE*, 16, e0251489, <https://doi.org/10.1371/journal.pone.0251489>,  
707 2021.

- 708 Calvin, K. and Bond-Lamberty, B.: Integrated human-earth system modeling—state of  
709 the science and future directions, *Environ. Res. Lett.*, 13, 063006,  
710 <https://doi.org/10.1088/1748-9326/aac642>, 2018.
- 711 Changming, L. and Shifeng, Z.: Drying up of the yellow river: its impacts and counter-  
712 measures, *Mitigation and Adaptation Strategies for Global Change*, 7, 203–214,  
713 <https://doi.org/10.1023/A:1024408310869>, 2002.
- 714 Cheng, Y., Huang, M., Lawrence, D. M., Calvin, K., Lombardozzi, D. L., Sinha, E.,  
715 Pan, M., and He, X.: Future bioenergy expansion could alter carbon sequestration  
716 potential and exacerbate water stress in the United States, *Science Advances*, 8,  
717 eabm8237, <https://doi.org/10.1126/sciadv.abm8237>, 2022.
- 718 Cobb, C. W. and Douglas, P. H.: A theory of production, *The American Economic*  
719 *Review*, 18, 139–165, 1928.
- 720 Cong, Z., Yang, D., Gao, B., Yang, H., and Hu, H.: Hydrological trend analysis in the  
721 Yellow River basin using a distributed hydrological model, *Water Resources Research*,  
722 45, 2008WR006852, <https://doi.org/10.1029/2008WR006852>, 2009.
- 723 Cui, T., Wang, Y., Sun, R., Qiao, C., Fan, W., Jiang, G., Hao, L., and Zhang, L.:  
724 Estimating Vegetation Primary Production in the Heihe River Basin of China with  
725 Multi-Source and Multi-Scale Data, *PLOS ONE*, 11, e0153971,  
726 <https://doi.org/10.1371/journal.pone.0153971>, 2016.
- 727 Davies, E. G. R. and Simonovic, S. P.: ANEMI: a new model for integrated assessment  
728 of global change, *Interdisciplinary Environmental Review*, 2011.
- 729 Di Vittorio, A. V., Sinha, E., Hao, D., Singh, B., Calvin, K. V., Shippert, T., Patel, P.,  
730 and Bond-Lamberty, B.: E3SM-GCAM: A Synchronously Coupled Human Component  
731 in the E3SM Earth System Model Enables Novel Human-Earth Feedback Research,  
732 *Journal of Advances in Modeling Earth Systems*, 17, e2024MS004806,  
733 <https://doi.org/10.1029/2024MS004806>, 2025.
- 734 Dobbs, G. R., Liu, N., Caldwell, P. V., Miniati, C. F., Sun, G., Duan, K., and Bolstad, P.  
735 V.: Inter-basin surface water transfers database for public water supplies in  
736 conterminous United States, 1986–2015, *Sci Data*, 10, 255,  
737 <https://doi.org/10.1038/s41597-023-02148-5>, 2023.
- 738 Dottori, F., Szewczyk, W., Ciscar, J.-C., Zhao, F., Alfieri, L., Hirabayashi, Y., Bianchi,  
739 A., Mongelli, I., Frieler, K., Betts, R. A., and Feyen, L.: Increased human and economic  
740 losses from river flooding with anthropogenic warming, *Nature Clim Change*, 8, 781–  
741 786, <https://doi.org/10.1038/s41558-018-0257-z>, 2018.
- 742 EEA: Trends in atmospheric concentrations of CO<sub>2</sub> (ppm), CH<sub>4</sub> (ppb) and N<sub>2</sub>O (ppb),

743 between 1800 and 2017, 2019.

744 Feng, X., Fu, B., Piao, S., Wang, S., Ciais, P., Zeng, Z., Lü, Y., Zeng, Y., Li, Y., Jiang,  
745 X., and Wu, B.: Revegetation in China's Loess Plateau is approaching sustainable water  
746 resource limits, *Nature Clim Change*, 6, 1019–1022,  
747 <https://doi.org/10.1038/nclimate3092>, 2016.

748 Feng, Y. and Zhu, A.: Spatiotemporal differentiation and driving patterns of water  
749 utilization intensity in Yellow River Basin of China: Comprehensive perspective on the  
750 water quantity and quality, *Journal of Cleaner Production*, 369, 133395,  
751 <https://doi.org/10.1016/j.jclepro.2022.133395>, 2022.

752 Flörke, M., Kynast, E., Bärlund, I., Eisner, S., Wimmer, F., and Alcamo, J.: Domestic  
753 and industrial water uses of the past 60 years as a mirror of socio-economic  
754 development: A global simulation study, *Global Environmental Change*, 23, 144–156,  
755 <https://doi.org/10.1016/j.gloenvcha.2012.10.018>, 2013.

756 Forrester, J. W.: *Principles of systems*, Pegasus Communications, Inc, Waltham, MA,  
757 1968.

758 Fu, B. and Li, Y.: Bidirectional coupling between the Earth and human systems is  
759 essential for modeling sustainability, *National Science Review*, 3, 397–398,  
760 <https://doi.org/10.1093/nsr/nww094>, 2016.

761 Fu, B., Liu, Y., Lü, Y., He, C., Zeng, Y., and Wu, B.: Assessing the soil erosion control  
762 service of ecosystems change in the Loess Plateau of China, *Ecological Complexity*, 8,  
763 284–293, <https://doi.org/10.1016/j.ecocom.2011.07.003>, 2011.

764 Fu, B., Liu, Y., and Meadows, M. E.: Ecological restoration for sustainable  
765 development in China, *National Science Review*, 10, nwad033,  
766 <https://doi.org/10.1093/nsr/nwad033>, 2023.

767 Fujimori, S., Masui, T., and Matsuoka, Y.: Development of a global computable general  
768 equilibrium model coupled with detailed energy end-use technology, *Applied Energy*,  
769 128, 296–306, <https://doi.org/10.1016/j.apenergy.2014.04.074>, 2014a.

770 Fujimori, S., Masui, T., and Matsuoka, Y.: Development of a global computable general  
771 equilibrium model coupled with detailed energy end-use technology, *Applied Energy*,  
772 128, 296–306, <https://doi.org/10.1016/j.apenergy.2014.04.074>, 2014b.

773 Fujimori, S., Wu, W., Doelman, J., Frank, S., Hristov, J., Kyle, P., Sands, R., van Zeist,  
774 W.-J., Havlik, P., Domínguez, I. P., Sahoo, A., Stehfest, E., Tabeau, A., Valin, H., van  
775 Meijl, H., Hasegawa, T., and Takahashi, K.: Land-based climate change mitigation  
776 measures can affect agricultural markets and food security, *Nat Food*, 3, 110–121,  
777 <https://doi.org/10.1038/s43016-022-00464-4>, 2022.

778 Gou, J., Miao, C., Samaniego, L., Xiao, M., Wu, J., and Guo, X.: CNRD v1.0: A High-  
779 Quality Natural Runoff Dataset for Hydrological and Climate Studies in China, *Bulletin*  
780 *of the American Meteorological Society*, 102, E929–E947,  
781 <https://doi.org/10.1175/BAMS-D-20-0094.1>, 2021.

782 Hasegawa, T., Sakurai, G., Fujimori, S., Takahashi, K., Hijioka, Y., and Masui, T.:  
783 Extreme climate events increase risk of global food insecurity and adaptation needs,  
784 *Nat Food*, 2, 587–595, <https://doi.org/10.1038/s43016-021-00335-4>, 2021.

785 Hyun, J.-Y., Huang, S.-Y., Yang, Y.-C. E., Tidwell, V., and Macknick, J.: Using a  
786 coupled agent-based modeling approach to analyze the role of risk perception in water  
787 management decisions, *Hydrology and Earth System Sciences*, 23, 2261–2278,  
788 <https://doi.org/10.5194/hess-23-2261-2019>, 2019.

789 Jain, S., Mindlin, J., Koren, G., Gulizia, C., Steadman, C., Langendijk, G. S., Osman,  
790 M., Abid, M. A., Rao, Y., and Rabanal, V.: Are We at Risk of Losing the Current  
791 Generation of Climate Researchers to Data Science?, *AGU Advances*, 3,  
792 e2022AV000676, <https://doi.org/10.1029/2022AV000676>, 2022.

793 Jia, K., Liang, S., Liu, S., Li, Y., Xiao, Z., Yao, Y., Jiang, B., Zhao, X., Wang, X., Xu,  
794 S., and Cui, J.: Global Land Surface Fractional Vegetation Cover Estimation Using  
795 General Regression Neural Networks From MODIS Surface Reflectance, *IEEE*  
796 *Transactions on Geoscience and Remote Sensing*, 53, 4787–4796,  
797 <https://doi.org/10.1109/TGRS.2015.2409563>, 2015.

798 Jia, K., Yang, L., Liang, S., Xiao, Z., Zhao, X., Yao, Y., Zhang, X., Jiang, B., and Liu,  
799 D.: Long-Term Global Land Surface Satellite (GLASS) Fractional Vegetation Cover  
800 Product Derived From MODIS and AVHRR Data, *IEEE Journal of Selected Topics in*  
801 *Applied Earth Observations and Remote Sensing*, 12, 508–518,  
802 <https://doi.org/10.1109/JSTARS.2018.2854293>, 2019.

803 Jiang, H., Simonovic, S. P., and Yu, Z.: ANEMI\_Yangtze v1.0: a coupled human–  
804 natural systems model for the Yangtze Economic Belt – model description, *Geosci.*  
805 *Model Dev.*, 26, 2022.

806 Kemei, Z., Rotich, T., and Bitok, J.: Modelling population dynamics using age-  
807 structured system of partial differential equations, *IJAMR*, 13, 110–116,  
808 <https://doi.org/10.14419/m81azj37>, 2024.

809 Li, M., Shan, R., Abdulla, A., Virguez, E., and Gao, S.: The role of dispatchability in  
810 China’s power system decarbonization, *Energy Environ. Sci.*, 17, 2193–2205,  
811 <https://doi.org/10.1039/D3EE04293F>, 2024.

812 Li, X., Cheng, G., Lin, H., Cai, X., Fang, M., Ge, Y., Hu, X., Chen, M., and Li, W.:

813 Watershed System Model: The Essentials to Model Complex Human-Nature System at  
814 the River Basin Scale, *Journal of Geophysical Research: Atmospheres*, 123, 3019–3034,  
815 <https://doi.org/10.1002/2017JD028154>, 2018.

816 Li, X., Zhang, L., Zheng, Y., Yang, D., Wu, F., Tian, Y., Han, F., Gao, B., Li, H., Zhang,  
817 Y., Ge, Y., Cheng, G., Fu, B., Xia, J., Song, C., and Zheng, C.: Novel hybrid coupling  
818 of ecohydrology and socioeconomy at river basin scale: A watershed system model for  
819 the Heihe River basin, *Environmental Modelling & Software*, 141, 105058,  
820 <https://doi.org/10.1016/j.envsoft.2021.105058>, 2021.

821 Li, Z., Liu, X., Niu, T., Kejia, D., Zhou, Q., Ma, T., and Gao, Y.: Ecological Restoration  
822 and Its Effects on a Regional Climate: The Source Region of the Yellow River, China,  
823 *Environ. Sci. Technol.*, 49, 5897–5904, <https://doi.org/10.1021/es505985q>, 2015.

824 Liu, C., Golding, D., and Gong, G.: Farmers’ coping response to the low flows in the  
825 lower Yellow River: A case study of temporal dimensions of vulnerability, *Global  
826 Environmental Change*, 18, 543–553, <https://doi.org/10.1016/j.gloenvcha.2008.09.002>,  
827 2008.

828 Liu, J.: Integration across a metacoupled world, *E&S*, 22, art29,  
829 <https://doi.org/10.5751/ES-09830-220429>, 2017.

830 Liu, J., Dietz, T., Carpenter, S. R., Alberti, M., Folke, C., Moran, E., Pell, A. N.,  
831 Deadman, P., Kratz, T., Lubchenco, J., Ostrom, E., Ouyang, Z., Provencher, W.,  
832 Redman, C. L., Schneider, S. H., and Taylor, W. W.: Complexity of Coupled Human  
833 and Natural Systems, *Science*, 317, 1513–1516,  
834 <https://doi.org/10.1126/science.1144004>, 2007.

835 Ministry of Agriculture and Rural Affairs of the People's Republic of China (MAARA),  
836 China Agriculture Yearbook,  
837 <https://doi.org/https://data.cnki.net/yearBook?type=type&code=A>, 2020.

838 Miao, C., Kong, D., Wu, J., and Duan, Q.: Functional degradation of the water–  
839 sediment regulation scheme in the lower Yellow River: Spatial and temporal analyses,  
840 *Science of The Total Environment*, 551–552, 16–22,  
841 <https://doi.org/10.1016/j.scitotenv.2016.02.006>, 2016.

842 Miao, C., Gou, J., Fu, B., Tang, Q., Duan, Q., Chen, Z., Lei, H., Chen, J., Guo, J.,  
843 Borthwick, A. G. L., Ding, W., Duan, X., Li, Y., Kong, D., Guo, X., and Wu, J.: High-  
844 quality reconstruction of China’s natural streamflow, *Science Bulletin*, 67, 547–556,  
845 <https://doi.org/10.1016/j.scib.2021.09.022>, 2022.

846 Monier, E., Paltsev, S., Sokolov, A., Chen, Y.-H. H., Gao, X., Ejaz, Q., Couzo, E.,  
847 Schlosser, C. A., Dutkiewicz, S., Fant, C., Scott, J., Kicklighter, D., Morris, J., Jacoby,

- 848 H., Prinn, R., and Haigh, M.: Toward a consistent modeling framework to assess multi-  
849 sectoral climate impacts, *Nat Commun*, 9, 1–8, [https://doi.org/10.1038/s41467-018-](https://doi.org/10.1038/s41467-018-02984-9)  
850 [02984-9](https://doi.org/10.1038/s41467-018-02984-9), 2018.
- 851 Motesharrei, S., Rivas, J., Kalnay, E., Asrar, G. R., Busalacchi, A. J., Cahalan, R. F.,  
852 Cane, M. A., Colwell, R. R., Feng, K., Franklin, R. S., Hubacek, K., Miralles-Wilhelm,  
853 F., Miyoshi, T., Ruth, M., Sagdeev, R., Shirmohammadi, A., Shukla, J., Srebric, J.,  
854 Yakovenko, V. M., and Zeng, N.: Modeling sustainability: population, inequality,  
855 consumption, and bidirectional coupling of the Earth and Human Systems, *National*  
856 *Science Review*, 3, 470–494, <https://doi.org/10.1093/nsr/nww081>, 2016.
- 857 National Bureau of Statistics of China (NBSC), *China Energy Statistical Yearbook*,  
858 <https://doi.org/https://data.cnki.net/yearBook?type=type&code=A>, 2020a.
- 859 National Bureau of Statistics of China (NBSC), *China Population Census Yearbook*,  
860 <https://doi.org/https://data.cnki.net/yearBook?type=type&code=A>, 2020b.
- 861 National Bureau of Statistics of China (NBSC), *China Statistical Yearbooks*,  
862 <https://doi.org/https://www.stats.gov.cn/english/>, 2020c.
- 863 Ning, X., Zhu, N., Liu, Y., and Wang, H.: Quantifying impacts of climate and human  
864 activities on the grassland in the Three-River Headwater Region after two phases of  
865 Ecological Project, *Geography and Sustainability*, 3, 164–176,  
866 <https://doi.org/10.1016/j.geosus.2022.05.003>, 2022.
- 867 Nordhaus, W. D.: Revisiting the social cost of carbon, *Proceedings of the National*  
868 *Academy of Sciences*, 114, 1518–1523, <https://doi.org/10.1073/pnas.1609244114>,  
869 2017.
- 870 Qu, W., Shi, W., Zhang, J., and Liu, T.: T21 China 2050: A Tool for National Sustainable  
871 Development Planning, *Geography and Sustainability*, 1, 33–46,  
872 <https://doi.org/10.1016/j.geosus.2020.03.004>, 2020.
- 873 Rajah, J. K., Blanz, B., Kopainsky, B., and Schoenberg, W.: An endogenous modelling  
874 framework of dietary behavioural change in the fully coupled human-climate FRIDA  
875 v2.1 model, *Geoscientific Model Development*, 18, 5997–6022,  
876 <https://doi.org/10.5194/gmd-18-5997-2025>, 2025.
- 877 Ren, M., Huang, C., Wu, Y., Deppermann, A., Frank, S., Havlík, P., Zhu, Y., Fang, C.,  
878 Ma, X., Liu, Y., Zhao, H., Chang, J., Ma, L., Bai, Z., Xu, S., and Dai, H.: Enhanced  
879 food system efficiency is the key to China’s 2060 carbon neutrality target, *Nat Food*, 4,  
880 552–564, <https://doi.org/10.1038/s43016-023-00790-1>, 2023.
- 881 Richardson, G. P.: Reflections on the foundations of system dynamics, *System*  
882 *Dynamics Review*, 27, 219–243, <https://doi.org/10.1002/sdr.462>, 2011.

883 Ristaino, J. B., Anderson, P. K., Bebber, D. P., Brauman, K. A., Cunniffe, N. J., Fedoroff,  
884 N. V., Finegold, C., Garrett, K. A., Gilligan, C. A., Jones, C. M., Martin, M. D.,  
885 MacDonald, G. K., Neenan, P., Records, A., Schmale, D. G., Tateosian, L., and Wei, Q.:  
886 The persistent threat of emerging plant disease pandemics to global food security,  
887 *Proceedings of the National Academy of Sciences*, 118, e2022239118,  
888 <https://doi.org/10.1073/pnas.2022239118>, 2021.

889 Rydzak, F., Obersteiner, M., Kraxner, F., Fritz, S., and McCallum, I.: FeliX3–Impact  
890 Assessment Model: Systemic View across Societal Benefit Areas beyond Global Earth  
891 Observation, Laxenburg: International Institute for Applied Systems Analysis (IIASA),  
892 2013.

893 Sang, S.: CHANS-SD-YRB V1.0: A System Dynamics model of the coupled human-  
894 natural systems for the Yellow River Basin (1.0.0),  
895 <https://doi.org/https://doi.org/10.5281/zenodo.17568963>, 2025.

896 Sang, S., Li, Y., Hou, C., Zi, S., and Lin, H.: The interprovincial green water flow in  
897 China and its teleconnected effects on the social economy, *Hydrol. Earth Syst. Sci.*, 29,  
898 67–84, <https://doi.org/10.5194/hess-29-67-2025>, 2025a.

899 Sang, S., Li, Y., Zong, S., Yu, L., Wang, S., Liu, Y., Wu, X., Song, S., Wang, X., and Fu,  
900 B.: The modeling framework of the coupled human and natural systems in the Yellow  
901 River Basin, *Geography and Sustainability*, 6, 100294,  
902 <https://doi.org/10.1016/j.geosus.2025.100294>, 2025b.

903 Shan, Y., Guan, D., Zheng, H., Ou, J., Li, Y., Meng, J., Mi, Z., Liu, Z., and Zhang, Q.:  
904 China CO2 emission accounts 1997–2015, *Sci Data*, 5, 170201,  
905 <https://doi.org/10.1038/sdata.2017.201>, 2018.

906 Song, S., Wen, H., Wang, S., Wu, X., Cumming, G. S., and Fu, B.: Quantifying the  
907 effects of institutional shifts on water governance in the Yellow River Basin: A social-  
908 ecological system perspective, *Journal of Hydrology*, 629, 130638,  
909 <https://doi.org/10.1016/j.jhydrol.2024.130638>, 2024.

910 Vaidyanathan, G.: Integrated assessment climate policy models have proven useful,  
911 with caveats, *Proc. Natl. Acad. Sci. U.S.A.*, 118, e2101899118,  
912 <https://doi.org/10.1073/pnas.2101899118>, 2021.

913 Ventana Systems, Inc.: Vensim DSS (version 9.3), 2023.

914 Verburg, P. H., Dearing, J. A., Dyke, J. G., Leeuw, S. van der, Seitzinger, S., Steffen,  
915 W., and Syvitski, J.: Methods and approaches to modelling the Anthropocene, *Global  
916 Environmental Change*, 39, 328–340, <https://doi.org/10.1016/j.gloenvcha.2015.08.007>,  
917 2016.

- 918 van Vliet, J.: Direct and indirect loss of natural area from urban expansion, *Nat Sustain*,  
919 2, 755–763, <https://doi.org/10.1038/s41893-019-0340-0>, 2019.
- 920 Waidelich, P., Batibeniz, F., Rising, J., Kikstra, J. S., and Seneviratne, S. I.: Climate  
921 damage projections beyond annual temperature, *Nat. Clim. Chang.*, 14, 592–599,  
922 <https://doi.org/10.1038/s41558-024-01990-8>, 2024a.
- 923 Waidelich, P., Batibeniz, F., Rising, J., Kikstra, J. S., and Seneviratne, S. I.: Climate  
924 damage projections beyond annual temperature, *Nat. Clim. Chang.*, 14, 592–599,  
925 <https://doi.org/10.1038/s41558-024-01990-8>, 2024b.
- 926 Wang, M., Sun, R., Zhu, A., and Xiao, Z.: Evaluation and Comparison of Light Use  
927 Efficiency and Gross Primary Productivity Using Three Different Approaches, *Remote*  
928 *Sensing*, 12, 1003, <https://doi.org/10.3390/rs12061003>, 2020a.
- 929 Wang, S., Fu, B., Piao, S., Lü, Y., Ciais, P., Feng, X., and Wang, Y.: Reduced sediment  
930 transport in the Yellow River due to anthropogenic changes, *Nature Geosci*, 9, 38–41,  
931 <https://doi.org/10.1038/ngeo2602>, 2016.
- 932 Wang, S., Song, S., Zhang, H., Yu, L., Jiao, C., Li, C., Wu, X., Zhao, W., Best, J.,  
933 Roberts, P., and Fu, B.: Anthropogenic impacts on the Yellow River Basin, *Nat Rev*  
934 *Earth Environ*, 6, 656–671, <https://doi.org/10.1038/s43017-025-00718-2>, 2025.
- 935 Wang, T., Teng, F., and Zhang, X.: Assessing global and national economic losses from  
936 climate change: a study based on CGEM-IAM in China, *Clim. Change Econ.*, 11,  
937 2041003, <https://doi.org/10.1142/S2010007820410031>, 2020b.
- 938 Wang, Y., Zhao, W., Wang, S., Feng, X., and Liu, Y.: Yellow River water rebalanced by  
939 human regulation, *Sci Rep*, 9, 9707, <https://doi.org/10.1038/s41598-019-46063-5>, 2019.
- 940 Wei, Z., Jian, Z., Sun, Y., Pan, F., Han, H., Liu, Q., and Mei, Y.: Ecological sustainability  
941 and high-quality development of the Yellow River Delta in China based on the  
942 improved ecological footprint model, *Sci Rep*, 13, 3821,  
943 <https://doi.org/10.1038/s41598-023-30896-2>, 2023.
- 944 Wu, J. and Gao, X.: Agridded daily observation dataset over China region and  
945 comparison with the other datasets, *Chinese Journal of Geophysics*, 56, 1102–1111,  
946 <https://doi.org/10.6038/cjg20130406>, 2013.
- 947 Wu, X., Yan, Z., Yang, H., Wang, S., Zhang, H., Shen, Y., Song, S., Liu, Y., Guo, Y.,  
948 Yang, D., and Fu, B.: Ecological restoration in the Yellow River Basin enhances  
949 hydropower potential, *Nat Commun*, 16, 2566, [https://doi.org/10.1038/s41467-025-](https://doi.org/10.1038/s41467-025-57891-7)  
950 [57891-7](https://doi.org/10.1038/s41467-025-57891-7), 2025.
- 951 Wu, Z., Li, Y., Wang, R., Xu, X., Ren, D., Huang, Q., Xiong, Y., and Huang, G.:

952 Evaluation of irrigation water saving and salinity control practices of maize and  
953 sunflower in the upper Yellow River basin with an agro-hydrological model based  
954 method, *Agricultural Water Management*, 278, 108157,  
955 <https://doi.org/10.1016/j.agwat.2023.108157>, 2023.

956 Xu, S., Wang, R., Gasser, T., Ciais, P., Peñuelas, J., Balkanski, Y., Boucher, O., Janssens,  
957 I. A., Sardans, J., Clark, J. H., Cao, J., Xing, X., Chen, J., Wang, L., Tang, X., and Zhang,  
958 R.: Delayed use of bioenergy crops might threaten climate and food security, *Nature*,  
959 609, 299–306, <https://doi.org/10.1038/s41586-022-05055-8>, 2022.

960 Xu, W., Xiao, Y., Zhang, J., Yang, W., Zhang, L., Hull, V., Wang, Z., Zheng, H., Liu, J.,  
961 Polasky, S., Jiang, L., Xiao, Y., Shi, X., Rao, E., Lu, F., Wang, X., Daily, G. C., and  
962 Ouyang, Z.: Strengthening protected areas for biodiversity and ecosystem services in  
963 China, *Proc. Natl. Acad. Sci. U.S.A.*, 114, 1601–1606,  
964 <https://doi.org/10.1073/pnas.1620503114>, 2017.

965 Xu, X., Liu, J., Zhang, S., Li, R., Yan, C., and Wu, S.: China land use remote sensing  
966 monitoring dataset, <https://doi.org/10.12078/2018070201>, 2018.

967 Yan, Z., Wang, T., Ma, T., and Yang, D.: Water-carbon-sediment synergies and trade-  
968 offs: Multi-faceted impacts of large-scale ecological restoration in the Middle Yellow  
969 River Basin, *Journal of Hydrology*, 634, 131099,  
970 <https://doi.org/10.1016/j.jhydrol.2024.131099>, 2024.

971 Yang, D., Shao, W., Yeh, P. J.-F., Yang, H., Kanae, S., and Oki, T.: Impact of vegetation  
972 coverage on regional water balance in the nonhumid regions of China, *Water Resources*  
973 *Research*, 45, <https://doi.org/10.1029/2008WR006948>, 2009.

974 Yang, Z., Li, Q., Xue, W., and Xu, Z.: Impacts of nature reserves on local residents’  
975 income in China, *Ecological Economics*, 199, 107494,  
976 <https://doi.org/10.1016/j.ecolecon.2022.107494>, 2022.

977 Ye, Q., Liu, Q., Swamy, D., Gao, L., Moallemi, E. A., Rydzak, F., and Eker, S.: FeliX  
978 2.0: An integrated model of climate, economy, environment, and society interactions,  
979 *Environmental Modelling & Software*, 179, 106121,  
980 <https://doi.org/10.1016/j.envsoft.2024.106121>, 2024.

981 Yin, P., Gao, Y., Chen, R., Liu, W., He, C., Hao, J., Zhou, M., and Kan, H.: Temperature-  
982 related death burden of various neurodegenerative diseases under climate warming: a  
983 nationwide modelling study, *Nat Commun*, 14, 8236, [https://doi.org/10.1038/s41467-](https://doi.org/10.1038/s41467-023-44066-5)  
984 [023-44066-5](https://doi.org/10.1038/s41467-023-44066-5), 2023a.

985 Yin, S., Gao, G., Ran, L., Lu, X., and Fu, B.: Spatiotemporal Variations of Sediment  
986 Discharge and In-Reach Sediment Budget in the Yellow River From the Headwater to

- 987 the Delta, *Water Resources Research*, 57, e2021WR030130,  
988 <https://doi.org/10.1029/2021WR030130>, 2021.
- 989 Yin, S., Gao, G., Ran, L., Li, D., Lu, X., and Fu, B.: Extreme streamflow and sediment  
990 load changes in the Yellow River Basin: Impacts of climate change and human activities,  
991 *Journal of Hydrology*, 619, 129372, <https://doi.org/10.1016/j.jhydrol.2023.129372>,  
992 2023b.
- 993 Yoon, J., Klassert, C., Selby, P., Lachaut, T., Knox, S., Avisse, N., Harou, J., Tilmant,  
994 A., Klauer, B., Mustafa, D., Sigel, K., Talozzi, S., Gawel, E., Medellín-Azuara, J.,  
995 Bataineh, B., Zhang, H., and Gorelick, S. M.: A coupled human–natural system analysis  
996 of freshwater security under climate and population change, *Proceedings of the*  
997 *National Academy of Sciences*, 118, e2020431118,  
998 <https://doi.org/10.1073/pnas.2020431118>, 2021.
- 999 Yellow River Conservancy Commission of the Ministry of Water Resources  
1000 (YRCCMWR), *Yellow River Basin Comprehensive Planning (2012-2030)*, 2015.
- 1001 Yellow River Conservancy Commission of the Ministry of Water Resources  
1002 (YRCCMWR), *Yellow River Water Resources Bulletin*, 2020.
- 1003 Yu, T., Sun, R., Xiao, Z., Zhang, Q., Liu, G., Cui, T., and Wang, J.: Estimation of Global  
1004 Vegetation Productivity from Global LAnd Surface Satellite Data, *Remote Sensing*, 10,  
1005 327, <https://doi.org/10.3390/rs10020327>, 2018.
- 1006 Zhang, H., Li, R., Cai, X., Zheng, C., Liu, L., Liu, M., Zhang, Q., Lin, H., Chen, L.,  
1007 and Wang, X.: Do electricity flows hamper regional economic–environmental equity?,  
1008 *Applied Energy*, 326, 120001, <https://doi.org/10.1016/j.apenergy.2022.120001>, 2022a.
- 1009 Zhang, Q., Gu, X., Singh, V. P., Kong, D., and Chen, X.: Spatiotemporal behavior of  
1010 floods and droughts and their impacts on agriculture in China, *Global and Planetary*  
1011 *Change*, 131, 63–72, <https://doi.org/10.1016/j.gloplacha.2015.05.007>, 2015.
- 1012 Zhang, T., Su, X., Zhang, G., Wu, H., and Liu, Y.: Projections of the characteristics and  
1013 probability of spatially concurrent hydrological drought in a cascade reservoirs area  
1014 under CMIP6, *Journal of Hydrology*, 613, 128472,  
1015 <https://doi.org/10.1016/j.jhydrol.2022.128472>, 2022b.
- 1016 Zhou, F., Bo, Y., Ciais, P., Dumas, P., Tang, Q., Wang, X., Liu, J., Zheng, C., Polcher,  
1017 J., Yin, Z., Guimberteau, M., Peng, S., Otle, C., Zhao, X., Zhao, J., Tan, Q., Chen, L.,  
1018 Shen, H., Yang, H., Piao, S., Wang, H., and Wada, Y.: Deceleration of China’s human  
1019 water use and its key drivers, *Proceedings of the National Academy of Sciences*, 117,  
1020 7702–7711, <https://doi.org/10.1073/pnas.1909902117>, 2020.
- 1021 Zhu, Y., Jia, X., Qiao, J., and Shao, M.: What is the mass of loess in the Loess Plateau

1022 of China?, Science Bulletin, 64, 534–539, <https://doi.org/10.1016/j.scib.2019.03.021>,  
1023 2019.

1024